Comparison of Aircraft Measurements during GoAmazon2014/5 and ACRIDICON-CHUVA

Fan Mei[1], Jian Wang[2], Jennifer M. Comstock[1], Ralf Weigel[13], Martina Krämer[14, 13], Christoph Mahnke[13, 8], John E. Shilling[1], Johannes Schneider[8], Christiane Schulz[8], Charles N. Long[7], Manfred Wendisch[5], Luiz A. T. Machado[3], Beat Schmid[1], Trismono Krisna[5], Mikhail Pekour[1], John Hubbe[1], Andreas Giez[6], Bernadett Weinzierl[6], Martin Zoeger[6], Mira L. Pöhlker[8], Hans Schlager[6], Micael A. Cecchini[9], Meinrat O. Andreae[8,10], Scot T. Martin[4], Suzane, S. de Sá[4], Jiwen Fan[1], Jason Tomlinson[1], Stephen Springston[2], Ulrich Pöschl[8], Paulo Artaxo[11], Christopher Pöhlker[8], Thomas Klimach[8] , Andreas Minikin[12], Armin Afchine[14], Stephan Borrmann[13,8]

1. Pacific Northwest National Laboratory, Richland, WA, United States.
2. Brookhaven National Laboratory, Upton, NY, United States.
3. National Institute for Space Research (INPE), São Paulo, Brazil
4. Harvard University, Cambridge, MA, United States
5. University of Leipzig, Leipzig, Germany
6. Deutsches Zentrum für Luft- und Raumfahrt (DLR), Oberpfaffenhofen, Germany
7. NOAA ESRL GMD/CIRES, Boulder, CO, United States
8. Max Planck Institute for Chemistry, Mainz, Germany
9. University of São Paulo (USP), São Paulo, Brazil
10. Scripps Institution of Oceanography, University of California San Diego, La Jolla, California, USA
11. Instituto de Física, Universidade de São Paulo, São Paulo, Brazil
12. DLR Oberpfaffenhofen, Flight Experiments Facility, Wessling, Germany
13. Institute for Physics of the Atmosphere, Johannes Gutenberg University, Mainz, Germany
14. Research Centre Jülich, Institute for Energy and Climate Research 7: Stratosphere (IEK-7), Jülich, Germany

Correspondence to: Fan Mei (fan.mei@pnnl.gov)

Abstract. The indirect effect of atmospheric aerosol particles on the Earth's radiation balance remains one of the most uncertain components affecting climate change throughout the industrial period. The large uncertainty is partly due to the incomplete understanding of aerosol-cloud interactions. One objective of the GoAmazon2014/5 and ACRIDICON-CHUVA projects was to understand the influence of the emissions from the tropical megacity of Manaus (Brazil) on the surrounding atmospheric environment of the rainforest and to investigate its role in the life cycle

of convective clouds. During one of the intensive observation periods (IOPs) in the dry season from September 1 to October 10, 2014, comprehensive measurements of trace gases and aerosol properties were carried out at several ground sites. In a coordinated way, the advanced suites of sophisticated in situ instruments were deployed aboard both the U.S. Department of Energy Gulfstream-1 (G1) aircraft and the German High Altitude and Long-Range Research Aircraft (HALO) during three coordinated flights on September 9, 21, and October 1. Here we report on the comparison of measurements collected by the two aircraft during these three flights. Such comparisons are challenging but essential for assessing the data quality from the individual platforms and quantifying their uncertainty sources. Similar instruments mounted on the G1 and HALO collected vertical profile measurements of aerosol particles number concentrations and size distribution, cloud condensation nuclei concentrations, ozone and carbon monoxide mixing ratios, cloud droplet size distributions, and downward solar irradiance. We find that the above measurements from the two aircraft agreed within the measurement uncertainties. The relative fraction of the aerosol chemical composition measured by instruments on HALO agreed with the corresponding G1 data, although the total mass loadings only have a good agreement at high altitudes. Furthermore, possible causes of the discrepancies between measurements on the G1 and HALO are examined in this paper. Based on these results, criteria for meaningful aircraft measurement comparisons are discussed.

1. Introduction

Dominated by biogenic sources, the Amazon basin is one of the few remaining continental regions where atmospheric conditions realistically represent those of the pristine or pre-industrial era (Andreae et al., 2015). As a natural climatic “chamber”, the area around the urban region of Manaus in central Amazonia is an ideal location for studying the atmosphere under natural conditions as well as under conditions influenced by human activities and biomass burning events (Andreae et al., 2015; Artaxo et al., 2013; Davidson et al., 2012; Keller et al., 2009; Kuhn et al., 2010; Martin et al., 2016b; Pöhlker et al., 2018; Poschl et al., 2010; Salati and Vose, 1984). The Observations and Modeling of the Green Ocean Amazon (GoAmazon2014/5) campaign was conducted in 2014 and 2015 (Martin et al., 2017; Martin et al., 2016b). The primary objective of GoAmazon2014/5 was to improve the quantitative understanding of the effects of anthropogenic

influences on atmospheric chemistry and aerosol-cloud interactions in the tropical rainforest area. During the dry season in 2014, the ACRIDICON (Aerosol, Cloud, Precipitation, and Radiation Interactions and Dynamics of Convective Cloud Systems)-CHUVA (Cloud Processes of the Main Precipitation Systems in Brazil) campaign also took place to study tropical convective clouds and precipitation over Amazonia (Wendisch et al., 2016).

A feature of the GoAmazon 2014/5 field campaign was the design of the ground sites' location, which uses principles of Lagrangian sampling to align the sites with the Manaus pollution plume (Figure 1: Source location – Manaus (T1 site), and downwind location – Manacapuru (T3 site)). The ground sites were overflown with the low-altitude U.S. Department of Energy (DOE) Gulfstream-1 (G1) aircraft and the German High Altitude and Long Range Research Aircraft (HALO). These two aircraft are among the most advanced in atmospheric research, deploying suites of sophisticated and well-calibrated instruments (Schmid et al., 2014; Wendisch et al., 2016). The pollution plume from Manaus was intensively sampled during the G1 and HALO flights and also by the DOE Atmospheric Radiation Measurement (ARM) program Mobile Aerosol Observing System and ARM Mobile Facility located at one of the downwind surface sites (T3 site- 70 km west of Manaus). The routine ground measurements with coordinated and intensive observations from both aircraft provided an extensive data set of multi-dimensional observations in the region, which serves i) to improve the scientific understanding of the influence of the emissions of the tropical megacity of Manaus (Brazil) on the surrounding atmospheric environment of the rainforest and ii) to understand the life cycle of deep convective clouds and study open questions related to their influence on the atmospheric energy budget and hydrological cycle.

As more and more data sets are merged to link the ground-based measurements with aircraft observations, and as more studies focus on the spatial variation and temporal evolution of the atmospheric properties, it is critical to quantify the uncertainty ranges when combining the data collected from the different platforms. Due to the challenges of airborne operations, especially when two aircraft are involved in data collection in the same area, direct comparison studies are rare. However, this type of research is critical for further combining the datasets between the ground sites and aircraft. Thus, the main objectives of the study herein are to demonstrate how to achieve meaningful comparisons between two moving platforms, to conduct detailed comparisons between data collected by two aircraft, to identify the potential measurement issues, to quantify

reasonable uncertainty ranges of the extensive collection of measurements, and to evaluate the measurement sensitivities to the temporal and spatial variance. The comparisons and the related uncertainty estimations quantify the current measurement limits, which provide realistic measurement ranges to climate models as initial conditions to evaluate their output.

The combined GoAmazon2014/5 and ACRIDICON-CHUVA field campaigns not only provide critical measurements of aerosol and cloud properties in an under-sampled geographic region but also offer a unique opportunity to understand and quantify the quality of these measurements using carefully orchestrated comparison flights. The comparisons between the measurements from similar instruments on the two research aircraft can be used to identify potential measurement issues and quantify the uncertainty range of the field measurements, which include primary meteorological variables (Section 3.1), trace gases concentrations (Section 3.2), aerosol particle properties (number concentration, size distribution, chemical composition, and microphysical properties) (Section 3.3), cloud properties (Section 3.4), and downward solar irradiance (Section 3.5). We evaluate the consistency between the measurements aboard the two aircraft for a nearly full set of gas, aerosol particle, and cloud variables. Results from this comparison study provide the foundation not only for assessing and interpreting the observations from multiple platforms (from the ground to low altitude, and then to high altitude) but also for providing high-quality data to improve the understanding of the accuracy of the measurements related to the effects of human activities in Manaus on local air quality, terrestrial ecosystems in rainforest, and tropical weather.

2. Measurements

2.1 Instruments

The ARM Aerial Facility deployed several in situ instruments on the G1 to measure atmospheric state parameters, trace gases concentrations, aerosol particle properties, and cloud characteristics (Martin et al., 2016b; Schmid et al., 2014). The instruments installed on HALO covered measurements of meteorological, chemical, microphysical, and radiation parameters. Details of measurements aboard HALO are discussed in the ACRIDICON-CHUVA campaign overview paper (Wendisch et al., 2016). The measurements compared between the G1 and HALO are listed in Table 1.

2.1.1 Atmospheric parameters

All G1 and HALO meteorological sensors were routinely calibrated to maintain measurement accuracy. The G1 primary meteorological data were provided at one-second time resolution based on the standard developed by the Inter-Agency Working Group for Airborne Data and Telemetry Systems (Webster and Freudinger, 2018). For static temperature measurement, the uncertainty given by the manufacturer (Emerson) is ±0.1 K, and the uncertainty of the field data is ±0.5 K. The static pressure had a measurement uncertainty of 0.5 hPa. The standard measurement uncertainties were ±2 K for the chilled mirror hygrometer and 0.5 ms^{-1} for wind speed.

On HALO, primary meteorological data were obtained from the Basic HALO Measurement and Sensor System (BAHAMAS) at one-second time resolution. The system acquired data from airflow and thermodynamic sensors and from the aircraft avionics and a high-precision inertial reference system to derive the basic meteorological parameters like pressure, temperature, the 3D wind vector, aircraft position, and attitude. Water vapor mixing ratio and further derived humidity quantities were measured by the Sophisticated Hygrometer for Atmospheric Research (SHARC) based on direct absorption measurement by a tunable diode laser (TDL) system. The absolute accuracy of the primary meteorological data was 0.5 K for air temperature, 0.3 hPa for air pressure, 0.4-0.6 ms^{-1} for wind, and 5% (±1 ppm) for water vapor mixing ratio. All sensors were routinely calibrated and traceable to national standards (Giez et al., 2017; Krautstrunk and Giez, 2012).

2.1.2 Gas phase

Constrained by data availability, this comparison of trace gas measurements is focused on carbon monoxide (CO) and ozone (O_3) concentrations. Those measurements were made aboard the G1 by a $CO/N_2O/H_2O$ instrument (Los Gatos Integrated Cavity Output Spectroscopy instrument model 907-0015-0001), and an Ozone Analyzer (Thermo Scientific, Model 49i), respectively. The G1 CO analyzer was calibrated for response daily by NIST-traceable commercial standards before the flight. Due to the difference between laboratory and field conditions, the uncertainty of the CO measurements is about ±5% for one-second sampling periods. An ultra-fast carbon monoxide monitor (Aero Laser GmbH, AL5002) was deployed on HALO. The detection of CO is based on a vacuum-ultraviolet-fluorimetry, employing the excitation of CO at 150 nm, and the precision is 2 ppb, and the accuracy is about 5%. The ozone analyzer measures ozone concentration based on the absorbance of ultraviolet light at a wavelength of 254 nm. The ozone analyzer (Thermo Scientific, Model 49c) in the HALO payload is very similar to the one on the

G1 (Model 49i), with an accuracy greater than 2 ppb or about ±5% for four-second sampling periods. The G1 ozone monitor was calibrated at the New York State Department of Environmental Conservation testing laboratory at Albany.

2.1.3 Aerosol

Aerosol number concentration was measured by different condensation particle counters (CPCs) on the G1 (TSI, CPC 3010) and HALO (Grimm, CPC model 5.410). Although two CPCs were from different manufacturers, they were designed using the same principle, which is to detect particles by condensing butanol vapor on the particles to grow them to a large enough size that they can be counted optically. Both CPCs were routinely calibrated in the lab and reported the data at one-second time resolution. The HALO CPC operated at 0.6-1 L min^{-1}, with a nominal cutoff of 4 nm. Due to inlet losses, the effective cutoff diameter increases to 9.2 nm at 1000 hPa, and 11.2 nm at 500 hPa (Andreae et al., 2018; Petzold et al., 2011). The G1 CPC operated at 1 L min^{-1} volumetric flow rate and the nominal cut-off diameter D_{50} measured in the lab was ~10 nm. During a flight, the cut-off diameter may vary due to tubing losses, which contributes less than 10 % uncertainty to the comparison between two CPC concentrations.

Two instruments deployed on the G1 measured aerosol particle size distribution. a Fast Integrated Mobility Spectrometer (FIMS) inside of the G1 cabin measured the aerosol mobility size from 15 to 400 nm (Kulkarni and Wang, 2006a, b; Olfert et al., 2008; Wang, 2009). The ambient aerosol particles were charged after entering the FIMS inlet and then separated into different trajectories in an electric field based on their electrical mobility. The spatially separated particles grow into super-micrometer droplets in a condenser where supersaturation of the working fluid is generated by cooling. At the exit of the condenser, a high-speed charge-coupled device camera captures the image of an illuminated grown droplet at high resolution. In this study, we used the FIMS 1 Hz data for comparison. The size distribution data from FIMS were smoothed. Aside from the FIMS, the airborne version of the Ultra High Sensitivity Aerosol Spectrometer (UHSAS) was deployed on G1 and HALO. The G1 and HALO UHSAS were manufactured by the same company, and both were mounted under the wing on a pylon. UHSAS is an optical-scattering, laser-based particle spectrometer system. The size resolution is around 5% of the particle size. The G1 UHSAS typically covered a size range of 60 nm to 1000 nm. HALO UHSAS covered 90 nm to 500 nm size range for the September 9 flight.

Based on operating principles, FIMS measures aerosol electrical mobility size and UHSAS measures the aerosol optical equivalent size. Thus, the difference in the averaged size distributions from those two types of instruments might be linked to differences in their underlying operating principles, such as the assumption in the optical properties of aerosol particles. The data processing in the G1 UHSAS assumed that the particle refractive index is similar to ammonium sulfate (1.55), which is larger than the average refractive index (1.41-0.013i) from a previous Amazon study (Guyon et al., 2003). The HALO UHSAS was calibrated with polystyrene latex spheres, which have a refractive index about 1.572 for the UHSAS wavelength of 1054 nm. The uncertainty due to the refraction index can lead to up to 10% variation in UHSAS measured size (Kupc et al., 2018). Also, the assumption of spherical particles affects the accuracy of UHSAS sizing of ambient aerosols.

The chemical composition of submicron non-refractory ($NR\text{-}PM_1$) organic and inorganic (sulfate, nitrate, ammonium) aerosol particles was measured using a high-resolution time-of-flight aerosol mass spectrometer (HR-ToF-AMS) aboard the G1 (DeCarlo et al., 2006; Jayne et al., 2000; Shilling et al., 2018; Shilling et al., 2013). Based on the standard deviation of observed aerosol mass loadings during filter measurements, the HR-ToF-AMS detection limits for the average time of thirteen seconds are approximately 0.13, 0.01, 0.02, 0.01 (3σ values) $\mu g\ m^{-3}$ for organic, sulfate, nitrate, and ammonium, respectively (DeCarlo et al., 2006). A Compact Time-of-flight Aerosol Mass Spectrometer (C-ToF-AMS) was operated aboard HALO to investigate the aerosol composition. Aerosol particles enter both the C-ToF-AMS and HR-ToF-AMS via constant pressure inlets controlling the volumetric flow into the instrument, although the designs of the inlets are somewhat different (Bahreini et al., 2008). The details about the C-ToF-AMS operation and data analysis are reported in Schulz's paper (Schulz et al., 2018). The overall accuracy has been reported as ~30 % for both AMS instruments (Alfarra et al., 2004; Middlebrook et al., 2012). Data presented in this section were converted to the same condition as the HALO AMS data, which is 995 hPa and 300 K. Both AMS instruments were calibrated before and after the field deployment and also once a week during the field campaign.

The number concentration of cloud condensation nuclei (CCN) was measured aboard both aircraft using the same type of CCN counter from Droplet Measurement Technologies (DMT, model 200). This CCN counter contains two continuous-flow, thermal-gradient diffusion chambers for measuring aerosols that can be activated at constant supersaturation. The

supersaturation is created by taking advantage of the different diffusion rates between water vapor and heat. After the supersaturated water vapor condenses on the CCN in the sample air, droplets are formed, counted, and sized by an Optical Particle Counter (OPC). The sampling frequency is one second for both deployed CCN counters. Both CCN counters were calibrated using ammonium sulfate aerosol particles in the diameter range of 20-200 nm. The uncertainty of the effective water vapor supersaturation was ±5%. (Rose et al., 2008)

2.1.4 Clouds

Aircraft-based measurements are an essential method for in situ samplings of cloud properties (Brenguier et al., 2013; Wendisch and Brenguier, 2013). Over the last 50–60 years, hot-wire probes have been the most commonly used devices to estimate liquid water content (LWC) in the cloud from research aircraft. Since the 1970s, the most widely used technique for cloud droplet spectra measurements has been developed based on the light-scattering effect. This type of instrument provides the cloud droplet size distribution as the primary measurement. By integrating the cloud droplet size distribution, additional information, such as LWC can be derived from the high-order data product.

Three cloud probes from the G1 are discussed in this manuscript. The Cloud Droplet Probe (CDP) is a compact, lightweight forward-scattering cloud particle spectrometer that measures cloud droplets in the 2 to 50 μm size range (Faber et al., 2018). Using state-of-the-art electro-optics and electronics, Stratton Park Engineering (SPEC Inc.) developed a Fast Cloud Droplet Probe (FCDP), which also use forward-scattering to determine cloud droplet distributions and concentrations in the same range as CDP with up to 100 Hz sampling rate. The G1 also carried a two-dimensional stereo probe (2DS, SPEC Inc.), which has two 128-photodiode linear arrays working independently. The 2DS electronics produce shadowgraph images with 10 μm pixel resolution. Two orthogonal laser beams cross in the middle of the sample volume, with the sample cross section for each optical path of 0.8 cm^2. The manufacturer claims the maximum detection size is up to 3000 μm for the 2DS. However, due to the counting statistic issue, the data used in this study is from 10–1000 μm only (Lawson et al., 2006). 2DS was upgraded with modified probe tips, and an arrival time algorithm was applied to the 2DS data processing. Both efforts effectively reduced the number of small (shattered) particles (Lawson, 2011). For G1 cloud probes, the

laboratory calibrations of the sample area and droplet sizing were performed before the field deployment. During the deployment, biweekly calibrations with glass beads were performed with the size variation of less than 5%, which were consistent with the pre-campaign and after-campaign calibrations. Comparison between the LWC derived from cloud droplet spectra with hot-wire LWC measurement was made to estimate/eliminate the coincidence errors in cloud droplet concentration measurements (Lance et al., 2010; Wendisch et al., 1996)

Aboard of HALO, two cloud probes were operated and discussed in this manuscript, each consisting of a combination of two instruments: Cloud Combination Probe (CCP) and a Cloud Aerosol Precipitation Spectrometer (CAPS, denoted as NIXE-CAPS; NIXE: Novel Ice Experiment). The CCP is a combination of a CDP (denoted as CCP-CDP) with a CIPgs (Cloud Imaging Probe with greyscale, DMT, denoted as CCP-CIPgs). NIXE-CAPS consists of a CAS-Dpol (Cloud and Aerosol Spectrometer, DMT, denoted as NIXE-CAS) and a CIPgs (denoted as NIXE-CIPgs). CIPgs is an optical array probe comparable to the 2DS operated on the G1. CIPgs obtains images of cloud elements using a 64-element photodiode array (15µm resolution) to generate two-dimensional images with nominal detection diameter size range from 15 to 960 µm (Klingebiel et al., 2015; Molleker et al., 2014).The CCP-CDP detects the forward-scattered laser light by cloud particles in the size range of 2.5 to 46 µm. The sample area of the CCP- CDP was determined to be 0.27±0.025 mm^2 with an uncertainty of less than 10% (Klingebiel et al., 2015). CAS-Dpol (or NIXE-CAS) is a light scattering probe comparable to the CDP but covers the size range of 0.6 to 50 µm in diameter, thus including the upper size range of the aerosol particle size spectrum (Luebke et al., 2016). Furthermore, CAS-Dpol measures the polarization state of the particles (Costa et al., 2017). Correspondingly to the G1 CDP, the performance of the CCP-CDP and NIXE-CAS were frequently examined by glass beads calibrations. Prior to or after each HALO flight, CCP-CIPgs and NIXE-CIPgs calibrations were performed by using a mainly transparent spinning disc that carries opaque spots of different but known size. The data of the CCP measured particle concentration on board of HALO are corrected to gain ambient conditions using a thermodynamic approach developed by (Weigel et al., 2016). For NIXE-CAPS, the size distributions were provided where NIXE-CAS was merged with the NIXE-CIPgs at 20 µm.

2.1.5 Solar radiation

The G1 radiation suite included shortwave (SW, 400 - 2,700 nm) broadband total upward and downward irradiance measurements using Delta-T Devices model SPN-1 radiometers. The radiation data were corrected for aircraft tilt from the horizontal reference plane. A methodology has been developed (Long; et al., 2010) for using measurements of total and diffuse shortwave irradiance and corresponding aircraft navigation data (latitude, longitude, pitch, roll, heading) to calculate and apply a correction for platform tilt to the broadband hemispheric downward SW measurements. Additionally, whatever angular offset there may be between the actual orientation of each radiometer's detector and what the navigation data say is level has also been determined for the most accurate tilt correction.

The Spectral Modular Airborne Radiation measurement sysTem (SMART-Albedometer) was installed aboard HALO. Depending on the scientific objective and the configuration, the optical inlets determining the measured radiative quantities can be chosen. The SMART-Albedometer has been utilized to measure the spectral upward and downward irradiances; thereby, it is called as an albedometer, as well as to measure the spectral upward radiance. The SMART-Albedometer is designed initially to cover measurements in the solar spectral range between 300 and 2,200 nm (Krisna et al., 2018; Wendisch et al., 2001; Wendisch et al., 2016). However, due to decreasing sensitivity of the spectrometer at large wavelengths, the use of the wavelengths was restricted to 300 – 1,800 nm. The spectral resolution is defined by the full width at half maximum (FWHM), which is between 2 and 10 nm. In this case, the instruments were mounted on an active horizontal stabilization system for keeping the horizontal position of the optical inlets during aircraft movements (up to +/- 6 degrees from the horizontal plane).

2.2 Flight patterns

During the dry season IOP (September 1 – October 10, 2014), two types of coordinated flights were carried out: one flight in cloud-free condition (September 9) and two flights with clouds present (September 21 and October 1). In this study, we compare the measurements for both coordinated flight patterns. The discussion is mainly focused on the flights under cloud-free conditions on September 9 and the flight with clouds present on September 21, as shown in figure 1. The other coordinated flight on October 1 is included in the supplemental document.

For the cloud-free coordinated flight, the G1 took off first and orbited around an area from the planned rendezvous point until HALO arrived in sight. It then coordinated with HALO and

performed a wing-to-wing maneuver along straight legs around 500 m above sea level, as shown in Figure 2. The normal G1 average sampling speed is 100 m s^{-1}, and the normal HALO average sampling speed is 200 m s^{-1}. During the coordinated flight on September 9, both aircraft also adjusted their normal sampling speed by about 50 m s^{-1} so that they could fly side by side.

For the second type of coordinated flights, the G1 and HALO flew the stacked pattern at their own typical airspeed. On September 21, the G1 also took off from the airport first, followed by HALO 15 minutes later. Then, both aircraft flew above the T3 ground site and subsequently flew several flight legs stacked at different altitudes. The two aircraft were vertically separated by about 330 m and sampled below, inside, and above clouds. Due to the different aircraft speeds, the time difference between two aircraft visiting the same part of the flight paths varied, increasing up to 1 hour at the end of the flight path, as shown in Figure 3. On October 1, the G1 focused on the cloud microphysical properties and contrasting polluted versus clean clouds. HALO devoted the flight to the cloud vertical evolution and life cycle and also probed the cloud processing of aerosol particles and trace gases. The G1 and HALO coordinated two flight legs between 950–1250 m above the T3 site under cloud-free conditions. Following that, HALO flew to the south of Amazonia, and the G1 continued sampling plume-influenced clouds above the T3 site, and then flew above the Rio Negro area.

In this study, to perform a meaningful comparison of in situ measurements, all the data from instruments were time-synchronized with the aircraft (G1 or HALO) navigation system. For AMS and CPC data, the time shifting due to tubing length and instrument flow had been corrected. For the coordinated flight on Sep. 9, the data compared was from the same type of measurements with the same sampling rate. For the measurements with the different sampling rate, the data were binned to the same time interval for comparison. For the flight with the cloud present (Sep.21 and Oct. 1), the following criteria are used: 1) the data collected by the two aircraft must be less than 30 mins apart from each other; 2) the comparison data were binned to 200 m altitude intervals; 3) the cloud flag was applied to the aerosol measurements, and the data affected by the cloud shattering are eliminated from the comparisons of aerosol measurements. Moreover, additional comparison criteria are specified for individual measurements in the following section. Table 2 shows the total number of points used for the comparison.

3. Results

3.1 Comparison of the G1 and HALO measurements of atmospheric state parameters

The atmospheric state parameters comprise primary variables observed by the research aircraft. The measurements provide essential meteorological information not only for understanding the atmospheric conditions but also for providing the sampling conditions for other measurements, such as those of aerosol particles, trace gases, and cloud microphysical properties.

For cloud-free coordinated flights, the comparison focused on the near side-by-side flight leg at around 500 m, as shown in Figure 2. Table 3 shows the basic statistics of the data for primary atmospheric state parameters, assuming that two measurements from the G1 and HALO have a proportional relationship without any offset (Y=m0*X). In general, the atmospheric state parameters observed from both aircraft were in excellent agreement. The linear regression achieved a slope that was near 1 for four individual measurements. The regression is evaluated using the equation below.

$$R^2 = 1 - \frac{SS_{regression}}{SS_{Total}} \quad (1)$$

Where the sum squared regression error is calculated by $SS_{regression} = \sum(y_i - y_{regression})^2$, and the sum squared total error is calculated by $SS_{Total} = \sum(y_i - \bar{y})^2$, y_i is the individual data point, $\bar{y}$ is the mean value, and $y_{regression}$ is the regression value. When the majority of the data points are in a narrow value range, using the mean is better than the regression line, and the R^2 will be negative (Neg in Table 3).

The difference between the average ambient temperatures on the two aircraft was 0.5 K, and the difference between the average dew point temperatures was about 1 K. For temperature and humidity, the G1 data were slightly higher than the HALO data. The main contributions to the observed differences include the error propagation in the derivation of the ambient temperature from the measured temperature, instrumental-measurement uncertainty, and the temporal and spatial variability. The average horizontal wind speed measured by HALO is 0.4 m s^{-1} higher than the average horizontal wind speed measured by the G1. The uncertainty source of wind estimation is mainly due to the error propagation from the indicated aircraft speed measurement and the aircraft ground speed estimation from GPS. The static pressure distribution measured aboard HALO showed a smaller standard deviation (0.9 hPa) compared to the value of the G1 (1.5 hPa). Part of the reason for this difference is a more substantial variation of the G1 altitude during level flight legs when the G1 flew at around 50 m/s higher than its normal airspeed. Thus, any biases

caused by their near side-by-side airspeeds being different from their typical airspeeds would be undetected during these coordinated flights.

For the coordinated flights under cloudy conditions, we used the criteria from Section 2 to compare ambient conditions measured by the G1 and HALO aircraft. In addition to the ordinary linear regression, we also used the orthogonal regression to minimize the perpendicular distances from the data points to the fitted line. The ordinary linear regression assumes only the response (Y) variable contains measurement error but not the predictor (X), which remains unknown when we start the comparison between the measurements from the G1 and HALO. Thus, the additional orthogonal regression exams the assumption in the least square regression and makes sure the roles of the variables have little influence on the results. In Table 4, two equations were used for the orthogonal regression. One assumes that two measurements have a proportional relationship (Y=m1*X). The other one assumes a linear relationship, which can be described with the slope-intercept equation Y=m*X+b. Two regression results in Table 4 doesn't show a significant difference. The regression using the slope-intercept equation shows a different level of improvement in each individual measurement and will be discussed in the corresponding sections.

As shown in Figure 4, the linear regression slopes for ambient temperature, dew point temperature, and pressure were also close to 1 between the G1 and HALO measurements during the September 21 coordinated flight. The R^2 value is also close to 1. These results suggest that the G1 and HALO measurements achieved excellent agreements. Note that the dew point temperature from the G1 measurement was erroneous and removed from the comparison the data points between 2200–2700 m and above 3700 m (Figure 4(c)) because the G1 sensor was skewed by wetting in the cloud. The HALO dew point temperature was calculated from the total water mixing ratio measured by TDL, and that measurement in the cloud was more accurate than the measurement made by the chilled mirror hydrometer aboard the G1.

The lower value of the R^2 value in horizontal wind speed means the ratio of the regression error and total error in wind measurement is much higher than the temperature and pressure measurements. The main contributions to this difference are the error propagation during the horizontal wind speed estimation and the temporal and spatial variance between two aircraft sampling location. We observed differences between the two aircraft data of up to 2 m s^{-1}, caused by the increasing sampling distance as the two aircraft were climbing up. For example, the G1 flew a level leg above T3 around 2500 m between 16:20-16:30, while HALO stayed around 2500

m for a short period and kept climbing to a higher altitude. Due to strong vertical motion, turbulence, and different saturations (evaporation-condensation processes), the variances in the horizontal wind speed (Figure 4(d)) were also more significant compared to the variances of temperature and pressure measurements.

3.2 Comparison of trace gas measurements

For the cloud-free coordinated flight, ozone is the only trace gas measurement available on both aircraft. The linear regression slope shows that the HALO ozone concentration was about 8% higher than the G1 concentration. The difference between the averaged ozone concentrations was 4.1 ppb. As mentioned in section 2.1.2, each instrument has a 2 ppb accuracy (or 5%) on the ground based on a direct photometric measurement measuring the ratio between a sample and ozone-free cell. The in-flight calibration suggested that the accuracy of each instrument could raise to 5-7% (or 2-3.5 ppb). Thus, the difference between the averaged ozone concentrations – 4.1 ppb is within the instrument variation. The primary source of bias is probably the different ozone loss in the sampling and transfer lines.

The comparison made on September 21 flight in Figure 5 shows good agreement for the vertically averaged ozone measurements. Comparing the statistics data from September 9, the ozone measurement is not sensitive to the temporal and spatial changes. Although we do not have the comparison data on September 9, the G1 and HALO CO measurements comparison shows a higher correlation than the ozone data comparison at different altitudes on September 21. Note that the data points with more substantial variance in CO concentration were excluded because the G1 and HALO were sampling different air masses between 2000-3000 m, as indicated in Figure S7. The CO plot in Figure (5b) shows the real atmospheric variability. Around 4000 ft, the CO reading from the G1 and HALO has the minimum variation and is averaged around 85 ppb, which is at the atmospheric background level. At lower altitudes and higher CO concentrations, the local contribution is not well-mixed, and the inhomogeneity expresses as the more substantial variations observed in the plot.

3.3 Comparison of aerosol measurements

Aerosol particles exhibited substantial spatial variations, both vertically and horizontally, due to many aerosol sources and complex atmospheric processes in the Amazon basin, especially with

the local anthropogenic sources in Manaus. Thus, spatially resolved measurements are critical to characterizing the properties of the Amazonian aerosols. The cloud-free coordinated flights allow us to compare the G1 and HALO aerosol measurements and thus will facilitate further studies that utilize the airborne measurements. The vertical profiles obtained using the G1 and HALO in different aerosol regimes of the Amazon basin have contributed to many studies (Fan et al., 2018; Martin et al., 2017; Wang et al., 2016).

The design and performance of the aircraft inlets can strongly influence measured aerosol particle number concentration, size distribution, and chemical composition (Wendisch et al., 2004). Therefore, they need to be taken into consideration when comparing the measurements aboard two aircraft. The G1 aerosol inlet is a fully automated isokinetic inlet. Manufacturer wind tunnel test and earlier studies show that this inlet operates for aerosol particles with diameter up to 5 μm, with transmission efficiency around 50 % at 1.5 μm (Dolgos and Martins, 2014; Kleinman et al., 2007; Zaveri et al., 2010). The HALO sub-micrometer Aerosol Inlet (HASI) was explicitly designed for HALO. Based on the numerical flow modeling, optical particle counter measurements, and field study evaluation, HASI has a cut-off size of 3 μm, with transmission efficiency larger than 90 % at 1 μm (Andreae et al., 2018; Minikin et al., 2017).

3.3.1 Aerosol particle number concentration

For the cloud-free coordinated flight, the linear regression of CPC and UHSAS between the G1 and HALO measurements are also included in Table 3. The total number concentration measured by HALO CPC was about 20 % lower than that by the G1 CPC, as shown in Figure 6 (a). The CPC measurement is critically influenced by the isokinetic inlet operation and performance. During the flights, the aircraft attitude, such as the pitch and roll angles will cause the isokinetic sampling under non-axial condition. The non-axial flow at the probe inlet may result in flow separation, turbulence, and particle deposition. Therefore, quantitative particle measurements have more substantial uncertainty. As shown in Figure 6 (b), we compared the CPC data by applying three different data quality criteria. The first criterion is the same criteria described in the previous section, and the linear regression is included in Table 3. The second criterion constrains the data under the isokinetic and iso-axial condition, and the plot in Figure 6(b) shows the iso-axial criteria reduced the broadness of the scattered data, but no significant change to the linear regression. We further constrained the data with the averaging. Based on the average wind speed and distance

between two aircraft, we averaged the data into 10 seconds interval and found that the regression R^2 increase to 0.9392. The typical uncertainty between two CPCs is 5-10% on the well-controlled environment.(Gunthe et al., 2009; Liu and Pui, 1974) Although both CPCs from the G1 and HALO were characterized in the lab to be within 10% with its respective lab standard, we observed 20% variance during the flight. This result suggests the challenging condition of airborne condition can significantly increase the systematic uncertainties of CPC measurements, such as systematic instrument drifts, different aerosol particle losses inside of the two CPCs, and different inlet transmission efficiencies in the two aircraft.

The CPC data in Figure 6 are color-coded with UTC time. The general trend is that the aerosol number concentration increased with time through the Manaus plume between 15:30 and 15:40. A similar trend was observed in aerosol particle number concentration (Figure 7) measured by the Ultra-High Sensitivity Aerosol Spectrometer (UHSAS)-Airborne version (referred to as UHSAS). The total number concentration data given by UHSAS (Figure 7) is integrated over the overlapping size range (90 – 500 nm for the September 9 flight) for both the G1 and HALO UHSAS. The linear regression shows that the total aerosol particle number concentration from HALO UHSAS is about 16.5% higher than that from the G1 UHSAS. The discrepancy between the two UHSAS measurements is mainly due to the error propagation in the sampling flow, the differential pressure transducer reading, the instrument stability, and calibration repeatability, consistent with the other UHSAS study (Kupc et al., 2018). In the airborne version of UHSAS, mechanical vibrations have a more significant impact on the pressure transducer reading than the case for the bench version of UHSAS.

For the coordinated flight on September 21, the G1 and HALO data are averaged to 200 m vertical altitude intervals (Figure 8). The data points with an altitude between 2000 – 3000 m altitude were excluded from the comparisons, because the G1 and HALO sampled different airmass, as evidenced from trace gas and aerosol chemical composition data (detailed in Section 3.2 and 3.3.3). The UHSAS size range was integrated from 100 to 700 nm on September 21. The variation of the size range was because the overlap of size distributions from both UHSAS instruments was changed. Both the CPC and UHSAS measurement comparisons show stronger variation at the low altitude, especially below 2000 m. Above 3500 m, the variations on the CPC and UHSAS measured concentration significantly smaller than the variation at the lower altitude. This result is consistent with the observation from the trace gas measurement and confirms that

the variability of aerosol properties changes significantly with time and space. It is noticeable that the discrepancy observed in the UHSAS measurements comparison is larger than that from the CPC comparison. That is because the aerosol flow control inside the UHSAS can't respond quickly enough to the rapid change of the altitude and caused significant uncertainty in the data.

3.3.2 Aerosol particle size distribution

For the cloud-free coordinated flight, the averaged aerosol size distributions measured by FIMS, G1 UHSAS, and HALO UHSAS during one flight leg are compared in Figure 9. For particle diameter below 90 nm, the G1 UHSAS overestimated the particle concentration, which is due to the uncertainty in counting efficiency correction. The UHSAS detection efficiency is close to 100% for particles larger than 100 nm and concentrations below 3000 cm^{-3} but decreases considerably for both smaller particles and higher concentrations (Cai et al., 2008). The aerosol counting efficiency correction developed under the lab conditions does not necessarily apply under the conditions during the flight. Between 90 nm and 250 nm, FIMS agreed well with the G1 UHSAS, whereas HALO UHSAS was about 30 % higher than the two instruments. For the size range of 250–500 nm, FIMS had good agreement with HALO UHSAS and was about 30-50 % higher than the G1 UHSAS depending on the particle size. Because the UHSAS has a simplified "passive" inlet, the large size aerosol particle loss in the UHSAS inlet was expected to increase with the increasing of the aircraft speed. Thus, the lower G1 UHSAS concentrations at a larger aerosol particle size are likely related to the particle loss correction.

For the September 21 flight, the vertical profiles of aerosol size distributions are averaged into 100 m altitude intervals (Figure 10). Overall, all size distribution measurements captured the mode near 100 nm between 800–1000 m at the top of the convective boundary layer, as indicated by the potential temperature (Figure 10(d)), which starts from a maximum near the ground and then becomes remarkably uniform across the convective boundary layer. The peak of the aerosol size distribution shifted from 100 nm to 150 nm with increasing altitude. Note that due to data availability, the aerosol size distribution data from the HALO UHSAS has a reduced vertical resolution.

3.3.3 Aerosol particle chemical composition

Figure 11 shows the vertical profiles of the aerosol mass concentrations measured by the two AMS on September 21. The upper panel shows the medians and interquartile ranges of the different species (organics, nitrate, sulfate, ammonium) and the total mass concentration for the G1 (circles) and HALO (triangles). The lower panel shows the difference between the medians of G1 and HALO. The error bars were calculated using error propagation from the error of the median (interquartile range divided by 2*sqrt(N)). The data were grouped into 400 m altitude bins. The total mass concentration is the highest in the lower altitudes between 100 m and 2000 m with a median value of 5 µg m^{-3} (G1-AMS). At altitudes between 2000 m and 3800 m, the aerosol mass concentration decreased to a median value of 1.2 µg m^{-3} (G1-AMS).

The most significant difference was observed at altitudes below 1800 m. The aerosol mass concentration measured by HALO-AMS is less than that measured by G1-AMS, likely due to particle losses in the constant pressure inlet (CPI) used on the HALO-AMS. Between 1800 m and 3000 m, the mass concentrations measured by the HALO-AMS exceed those measured by the G1-AMS. This is most likely because the G1 was sampling different air masses than the HALO as indicated by the differences in CO mixing ratios and the CPC concentrations for this altitude region (see Fig. 5 and 8). Above 3000 m altitude, both instruments agree within the uncertainty range.

Among individual species, the largest difference above 2000 m is observed for ammonium. The deployed G1 AMS is a high-resolution mass spectrometer (HR-ToF), whereas the HALO-AMS has a lower resolution (C-ToF). The higher resolution of the G1-AMS allows for a better separation of interfering ions at m/z 15, 16, and 17 (NH+, NH2+, NH3+) and thereby a more reliable calculation of the ammonium mass concentration.

Overall the aerosol chemical composition is dominated by organics, as is evident from the vertical profiles of the relative fractions (Fig. 12). Both AMS show a dominant contribution of organics to the total mass concentration with values around 70 %. This contribution is constant at altitudes between 100 m and 3500 m and decreases to 50 % at 3800 m altitude. The inorganic fraction has the highest contribution from sulfate (20 %), followed by ammonium (7 %) and nitrate (2 – 4 %). For organics, ammonium, and sulfate both instruments give similar relative fractions, only for nitrate where a discrepancy is observed between 1000 and 3000 m. Although the absolute aerosol mass concentration measured by the HALO-AMS was affected by the constant pressure inlet below 1800 m altitude, the relative fractions of both instruments generally agree well. Similar

results were found for a second comparison flight on October 1, 2014 (see supplemental plots S13, S14).

3.3.4 CCN number concentration

These measurements provide key information about the aerosol's ability to form cloud droplets and thereby modify the microphysical properties of clouds. Numerous laboratory and field studies have improved the understanding of the connections among aerosol particle size, chemical composition, mixing states and CCN activation properties (Bhattu and Tripathi, 2015; Broekhuizen et al., 2006b; Chang et al., 2010; Duplissy et al., 2008; Lambe et al., 2011; Mei et al., 2013a; Mei et al., 2013b; Pöhlker et al., 2016; Thalman et al., 2017). In addition, based on the simplified chemical composition and internal mixing state assumption, various CCN closure studies have achieved success within ±20% uncertainty for ambient aerosols (Broekhuizen et al., 2006a; Mei et al., 2013b; Rissler et al., 2004; Wang et al., 2008).

According to earlier studies (Gunthe et al., 2009; Pöhlker et al., 2016; Roberts et al., 2001; Roberts et al., 2002; Thalman et al., 2017), the hygroscopicity (κ_{CCN}) of CCN in the Amazon basin is usually dominated by organic components (κ_{Org}). Long-term ground-based measurements at the Amazon Tall Tower Observatory also suggest low temporal variability and lack of pronounced diurnal cycles in hygroscopicity only under natural rainforest background conditions (Pöhlker et al., 2018; Pöhlker et al., 2016).

Using FIMS and CCN data from both the G1 and HALO collected during the coordinated flight leg on September 9, the critical activation dry diameter (D_{50}) was determined by integrating FIMS size distribution to match the CCN total number concentration. Then, the effective particle hygroscopicity was derived from D_{50} and the CCN-operated supersaturation using the κ-Köhler theory. The histogram plots based on the density of the estimated hygroscopicity (κ_{est}) from both aircraft were compared for the flight leg above T3. The κ_{est} values derived from the G1 and HALO measurements during the flight leg above the T3 site are 0.19±0.07 and 0.19±0.08, respectively. Those values agree very well with the overall mean value of 0.17±0.06derived from long-term measurements at the Amazon Tall Tower Observatory (Pöhlker et al., 2016; Thalman et al., 2017).

A comparison of the vertical profiles of the CCN concentrations at 0.5% supersaturation on September 21 is shown in Figure 13 as an example. The difference between the CCN measurements on the two aircraft is about 20% on average. The linear regression slope would increase to 0.9120 if we focused on the data above 2500 m. The main contributions to the difference include the difference in aerosol inlet structure, aerosol particle loss correction in the main aircraft inlet and the constant pressure inlet, the systematic inlet difference below 2500 m as shown in AMS data, as well as the error propagation of CCN measurements.

3.4 Comparison of cloud measurements

In situ cloud measurements help to capture the diversity of different cloud forms and their natural temporal and spatial variability. The G1 CDP and FCDP were deployed under the different wing pylons, and also on the different side of the aircraft. The G1 2DS was deployed on the same side of FCDP. The HALO cloud combination probe (CCP-CDP and CCP-CIPgs) and NIXE-CAPS (NIXE-CAS and NIXE-CIPgs) were deployed under the different wing pylons but on the same side of the aircraft. On September 21, 2014, based on the aircraft location and elevation information as shown in Figure 1(b) and Figure 3, two aircraft were sampling above T3 site and passing through the same cloud field at ~1600 m flight leg and ~1900 m flight leg as shown in Figure S8 and Figure S9. We used the cloud probes data from ~1900 m flight leg for the cloud droplet number concentration comparison. Two size ranges were considered: 3-20 μm from light scattering probes (CDP vs. FCDP on the G1, CCP-CDP vs. NIXE-CAS on HALO) and 2-960 μm from combined cloud probes.

3.4.1 Comparison of cloud droplet number concentration between 3-20 μm

For underwing cloud probes, such as the CDP and the CAS, Lance (Lance, 2012) suggests an undercounting bias of measured particle number concentration by up to 44% due to coincidence as soon as the ambient cloud particle density rises to 1000 per cm^3. At identical cloud particle densities, an earlier study (Baumgardner et al., 1985) estimates the coincidence bias for underwing cloud probes to the range at 20%. Factually, the coincidence correction depends on the instruments' individual detection volume, the air's volume flow rate through the detector and the cloud particles' residence time within the detection volume (Hermann and Wiedensohler, 2001; Jaenicke, 1972). For this comparison, coincidence bias remained unconsidered for each of the

cloud probe measurements to avoid deviations that are caused by the application of different corrections.

The primary cloud layer was observed by both the G1 and HALO between 1000-2500 m above ground. Although the two aircraft have sampled along the same flight path, the instruments probably observed different sets of the cloud due to cloud movement with the prevailing wind or different cloud evolution stages. Thus, an initial comparison focuses on the redundant instruments on the same aircraft, that measured truly collocated and synchronous on board of HALO and of the G1, respectively. In Figure 14 (a), the data of the CCP-CDP and of the NIXE-CAS are juxtaposed sampled over about 13 minutes for particles detection size ranges which were considered as most equivalent. The comparison reveals two ranges of particle number concentrations at which densification of agreeing measurements become visible. At very low number concentrations (about 10^{-1} – 10 per cm³) the presence of inactivated (interstitial) aerosols in the clear air space between the very few cloud elements should be considered. Over specific ranges, however, the fine structure of varying cloud droplet number concentration may cause the regression's scattering, indicated by cloud particle measured by one instrument whilst respective antagonist seems to measure within almost clear air – and vice versa. At higher number concentrations, i.e., between 10^2 and 10^3 per cm³, the comparison of the highly resolved data constitutes increasing compactness with respect to the 1:1 line. The overall data scatter of this comparison, however, may indicate the highly variable structure within clouds as those investigated over the Amazon basin. The data of the G1 CDP and the FCDP are juxtaposed as the same as HALO cloud probes. However, the sampled cloud period was much shorter – about 3 minutes. Similar to the HALO cloud probes comparison, we observe two ranges of particle number concentrations at which densification of agreeing measurements become visible, especially for the lower number concentrations (Figure 14(b)). At higher number concentrations, only a few cloud elements were observed by the G1 cloud probes. That is because the G1 was about 7-23 minutes later to pass the same location as HALO, and experienced much fewer cloud elements.

3.4.2 Comparison of cloud droplet size distribution between 2-960 μm from both aircraft

Comparing the cloud probes from the G1 and HALO, the size distributions from the HALO CCP and NIXE-CAPS probes are in remarkably good agreement between 2-960 μm, and both

peaked around 10 μm, as shown in Figure 15. That is because the potential effects of cloud elements' shattering on the probe measurements were considered similarly for the HALO-deployed CCP and NIXE instruments. On the G1, the CDP and FCDP had a more significant difference in the size range less than 8 μm, although both of them peaked between 10-20 μm. The difference between the G1 CDP and FCDP is mainly due to the data post-processing. The G1 CDP used an old data acquisition system from the Science engineering Associates, which limited its capability to store the particle-by-particle (PBP) data for further processing. CDP had placed an 800-μm-diameter pinhole in front of the sizing detector to minimize the coincidence up to 1850 cm^{-3}. On the other side, FCDP was equipped with new electronics and PBP data was locally stored in a flash drive onboard the Linux machine. For the G1 flights, a constant probe-dependent adjustment factor was applied to FCDP to adjust the coincidence further. The G1 CDP and FCDP operated with a redesigned probe tip to minimize the shattering effect. An additional algorithm was applied to the FCDP data to eliminate particles with short interarrival times.

For cloud droplets larger than 20 μm, the difference between the obtained cloud particle size distributions from two aircraft becomes substantial (up to two orders of magnitude) which indicated the observations of two different stages within the progressing development of a precipitation cloud. The precipitation cloud developing process is evidently expressed in elevated number concentrations of larger cloud elements observed during the G1 measurement that happened later. We also observed that the general cloud characteristic is similar at different altitude levels, as shown in Figure S10. The first two of three averaged periods were chosen during the flight leg of ~1600 m and the last average period is for the flight leg ~1900 m compared in Figure 15. Due to the averaging, the fine in-cloud structure gets suppressed. The small scale variabilities inside a cloud which are illustrated by the scattering of the highly resolved measurement data from the instrument comparison (cf. Figure 14) and the temporal evolution of in-cloud microphysics are not ascertainable and furthermore are beyond the scope of this study.

3.5 Comparison of radiation measurements

In this study, the downward irradiance measured by the SPN-1 unshaded center detector was compared with the integrated downward irradiance from the SMART-Albedometer between 300–1,800 nm wavelengths in Figure 16. Only measurements from flight legs, where the G1 and

HALO flew near side-by-side and at the same altitude were taken into consideration for analysis. In Figure 16, the top panel shows the time series of SPN-1 measurements, and the bottom panel shows the time series of SMART-Albedometer measurements. The black dots represented all data, and the blue circles identified data when the navigation condition was within +/- 1 degree from the horizontal level. The large scatter in the data between 15:12-15:28 and 15:35-15:40 is mainly due to the different sensor trajectories during the maneuvering of the aircraft to get to the coordinated flight position. Because of the difference of each aircraft position from horizontal, the measured signal varied from the signal of the direct component of sunlight. Each sensor might look at different directions of the sky or different parts of the clouds. In addition, both aircraft flew under scattered clouds, and this uneven sunlight blocking is another contribution to the "drop-off" behavior in the time series plots of the downward irradiance.

Comparing the G1 and HALO measurements between 15:15-1:55 using the restricted navigation criteria in Figure S15, we observed that the G1 SPN1 irradiance is slightly higher than the integrated irradiance from the SMART-Albedometer. We estimated the weighted irradiance using the NCAR tropospheric ultraviolet and visible (TUV) radiation model (at 15:42:00 on Sep 9, 2014) and confirmed that the spectral variation in the instruments is the main contribution to the difference in the comparison.

4 Uncertainty assessment

As mentioned in the introduction, a low-flying G1 and a high-flying HALO cover the sampling area from the atmospheric boundary layer to the free troposphere, and the sampling period from the dry and wet seasons (Martin et al., 2016a). This spatial coverage provides the user community with abundant atmospheric-related data sets for their further studies, such as for remote sensing validation and modeling evaluation. However, one critical step to bridge the proper usage of the observation with further atmospheric science study is to understand the measurement uncertainty in this data set, especially the variation between the coexisting measurements due to the temporal and spatial difference.

For the majority of the measurements during this field study, three primary sources contribute to the measurement variation between the two aircraft: the temporal and spatial variations, the difference in the inlet characterization, and the limitation of the instrument capability. We used

683 both ordinary least squares (OLS) linear regression and the orthogonal distance regression (ODR)
684 to correlate the measurements from the G1 and HALO and confirmed that the slope and R^2 are
685 very similar for the measurements made on September 9. The results from Table 2 confirmed that
686 the G1 and HALO measurements should be in a linear relationship without an offset if there is no
687 altitude variation. It also shows the minimum discrepancy between two aerosol instruments (CPC
688 or UHSAS) could be around 20%, which will include the error caused by the difference in the inlet
689 characterization and the limitation of the instrument capability. If we assume those two
690 measurement variation sources are not affected by the altitude, then by comparing the linear
691 regression data from Table 3 to Table 2, we can estimate the temporal and spatial variation between
692 two aircraft in a stack flight pattern. Three linear regression approaches were assessed, and the
693 results are listed in Table 3. If we assume that two measurements from the G1 and HALO should
694 not have any offsets, the OLS and ODR regressions show similar results. For the meteorological
695 parameters, this assumption is valid. In addition, good correlations also indicate that there is no
696 significant temporal or spatial variation during the stack pattern flight. As expected, the wind speed
697 and the aerosol measurements show that the correlations between the measurements from the G1
698 and HALO significantly improved with the offset assumption. This result suggests that the
699 temporal and spatial variation in a half-hour will add an additional 20% variance to the measured
700 aerosol properties. This will lead a considerable uncertainty when we combine the observation
701 data between the ground station and airborne platform. Thus, more routine and long-term airborne
702 measurements should be used to evaluate or constrain atmospheric modeling work.

703

704 ## 5 Summary

705 In situ measurements made by well-characterized instruments installed on two research aircraft
706 (the G1 and HALO) during the GoAmazon 2014/5 and ACRIDICON-CHUVA campaigns were
707 compared. Overall, the analysis shows good agreement between the G1 and HALO measurements
708 for a relatively broad range of atmospheric-related variables in a challenging lower troposphere
709 environment. Measured variables included atmospheric state parameters, aerosol particles, trace
710 gases, clouds, and radiation properties. This study outlines the well-designed coordinated flights
711 for achieving a meaningful comparison between two moving platforms. The high data quality was
712 ensured by the most sophisticated instruments aboard two aircraft used the most advanced

techniques, assisted with the best-calibrated/characterized procedures. The comparisons and the related uncertainty estimations quantify the current measurement limits, which provide the guidance to the modeler to realistically quantify the modeling input value and evaluate the variation between the measurement and the model output. The comparison also identified the measurement issues, outlined the associated reasonable measurement ranges, and evaluated the measurement sensitivities to the temporal and spatial variance.

The comparisons presented here were mainly from two coordinated flights. The flight on September 9 was classified as a cloud-free flight. During this flight, the G1 and HALO flew nearly side-by-side within a "polluted" leg, which was above the T3 site and across the downwind pollution plume from Manaus, and a "background" leg, which was outbound from Manaus to the west and could be influenced by the regional biomass burning events during the dry season. Both legs were at 500 m altitude and showed linear regression slopes of ambient temperature and pressure, horizontal wind speed and dew point temperature near to 1 between the G1 and HALO measurements. These comparisons provide a solid foundation for further evaluation of aerosol, trace gas, cloud, and radiation properties. The total aerosol concentration from CPC and UHSAS were compared for the 500 m flight leg above the T3 site. The UHSAS measurement had a better agreement than the CPC measurement. That is because of the minor difference in the inlet structure and instrument design between two UHSAS aboard the two aircraft. The average size distribution from both UHSAS and one FIMS in the G1 suggests that UHSAS had an over-counting issue at the size range between 60-90 nm, which was probably due to electrical noise and small signal-to-noise ratio in that size range. Good agreement in the aerosol size distribution measurement provides a "sanity" check for AMS measurements. A CCN closure study suggested that FIMS provides valuable size coverage for better CCN number concentration estimation. Based on the κ-Köhler parameterization, κ_{est} observed at 500 m above the T3 site is 0.19±0.08, which is similar to the overall mean kappa from long-term ATTO measurements - 0.17±0.06 (Pöhlker et al., 2016). This similarity suggests that there is no significant spatial variability along the downwind transect, although the freshly emitted aerosol particles may have much less hygroscopicity. The difference in the ozone measurement comparison is about 4.1 ppb, which suggests that the bias due to the sampling line loss inside of the G1 gas inlet. The irradiance from the SPN1 unshaded center detector in the G1 was compared with the HALO integrated downward irradiance between 300–1800 nm and achieved a very encouraging agreement with a variance of less than 10%.

744 During the second type of the coordinated flights on September 21 (with cloudy conditions),
745 HALO followed the G1 after take-off from Manus airport; then the two aircraft flew stacked legs
746 relative to each other at different altitudes above the T3 site. For atmospheric state parameters,
747 nearly linear correlations between the G1 and HALO were observed for ambient pressure,
748 temperature, and dew point temperature measurements at an altitude range from ground to around
749 5000 m. The horizontal wind had more variation than the rest of the meteorological properties,
750 which is mainly due to the temporal and spatial variability. The aerosol number concentration
751 comparison confirms that inhomogeneous aerosol distribution observed by the trace gas
752 measurements. The integrated aerosol number concentration from UHSAS showed consistent
753 discrepancy at different altitudes. This considerable uncertainty in the UHSAS measurements is
754 caused by the significant aerosol flow variations due to the slow and unstable flow control.
755 Although the aircraft-based UHSAS is a challenging instrument to operate, a reasonable size
756 distribution profile comparison was made between both UHSAS and FIMS on the G1. Overall the
757 chemical composition of the aerosol is dominated by organics. Around 70% organic contribution
758 maintains constant up to 3500 m, then decreases to 50%. The most substantial difference among
759 all the species is observed for ammonium due to the different resolution, and more reliable
760 ammonium mass concentration can be achieved with high resolution mass spectrometer. Although
761 the absolute aerosol mass concentration measured by the HALO AMS was affected below 1800
762 m altitude by the constant pressure inlet, the relative fractions of both instruments from the G1 and
763 HALO agree well.

764 Cloud probe comparisons were made for the cloud droplet number concentration between 3–
765 20 μm for the initial comparison between the redundant instruments on the same aircraft. Then the
766 comparison of cloud droplet size distribution between 2-960 μm for a flight leg around 1900 m
767 showed a remarkably good agreement. The major cloud appearance was captured by both aircraft,
768 although the cloud elements observed were affected by the cloud movement with the prevailing
769 wind and the different cloud evolution stages. Furthermore, the relatively short time delay of 7-23
770 minutes between the independent measurements may give a hint for the time scales in which the
771 cloud droplet spectra develop within a convective cloud over the Amazon basin.

772 The above results provide additional information about the reasonableness of measurements
773 for each atmospheric variable. This study confirms the high-quality spatial and temporal dataset

with clearly identified uncertainty ranges had been collected from two aircraft and builds a good foundation for further studies on the remote sensing validation and the spatial and temporal evaluation of modeling representation of the atmospheric processing and evolution.

Acknowledgments: This study was supported by the U.S. DOE, Office of Science, Atmospheric System Research Program, and used data from Atmospheric Radiation Measurement Aerial Facility, a DOE Office of Science User Facility. The Pacific Northwest National Laboratory (PNNL) is operated for DOE by Battelle under contract DE-AC05-76RL01830. This work was also supported by the Max Planck Society, the DFG (Deutsche Forschungsgemeinschaft, German Research Foundation) HALO Priority Program SPP 1294, the German Aerospace Center (DLR), the FAPESP (São Paulo Research Foundation) Grants 2009/15235-8 and 2013/05014-0, and a wide range of other institutional partners. The contributions from Micael A. Cecchini were funded by FAPESP grant number 2017/04654-6.

References:

Alfarra, M. R., Coe, H., Allan, J. D., Bower, K. N., Boudries, H., Canagaratna, M. R., Jimenez, J. L., Jayne, J. T., Garforth, A. A., and Li, S.-M.: Characterization of urban and rural organic particulate in the lower Fraser valley using two aerodyne aerosol mass spectrometers, Atmos Environ, 38, 5745-5758, 2004.

Andreae, M. O., Acevedo, O. C., Araujo, A., Artaxo, P., Barbosa, C. G. G., Barbosa, H. M. J., Brito, J., Carbone, S., Chi, X., Cintra, B. B. L., da Silva, N. F., Dias, N. L., Dias, C. Q., Ditas, F., Ditz, R., Godoi, A. F. L., Godoi, R. H. M., Heimann, M., Hoffmann, T., Kesselmeier, J., Konemann, T., Kruger, M. L., Lavric, J. V., Manzi, A. O., Lopes, A. P., Martins, D. L., Mikhailov, E. F., Moran-Zuloaga, D., Nelson, B. W., Nolscher, A. C., Nogueira, D. S., Piedade, M. T. F., Pohlker, C., Poschl, U., Quesada, C. A., Rizzo, L. V., Ro, C. U., Ruckteschler, N., Sa, L. D. A., Sa, M. D., Sales, C. B., dos Santos, R. M. N., Saturno, J., Schongart, J., Sorgel, M., de Souza, C. M., de Souza, R. A. F., Su, H., Targhetta, N., Tota, J., Trebs, I., Trumbore, S., van Eijck, A., Walter, D., Wang, Z., Weber, B., Williams, J., Winderlich, J., Wittmann, F., Wolff, S., and Yanez-Serrano, A. M.: The Amazon Tall Tower Observatory (ATTO): overview of pilot measurements on ecosystem ecology, meteorology, trace gases, and aerosols, Atmos Chem Phys, 15, 10723-10776, 2015.

Andreae, M. O., Afchine, A., Albrecht, R., Holanda, B. A., Artaxo, P., Barbosa, H. M. J., Borrmann, S., Cecchini, M. A., Costa, A., Dollner, M., Fütterer, D., Järvinen, E., Jurkat, T., Klimach, T., Konemann, T., Knote, C., Krämer, M., Krisna, T., Machado, L. A. T., Mertes, S., Minikin, A., Pöhlker, C., Pöhlker, M. L., Pöschl, U., Rosenfeld, D., Sauer, D., Schlager, H., Schnaiter, M., Schneider, J., Schulz, C., Spanu, A., Sperling, V. B., Voigt, C., Walser, A., Wang, J., Weinzierl, B., Wendisch, M., and Ziereis, H.: Aerosol characteristics and particle production in the upper troposphere over the Amazon Basin, Atmos. Chem. Phys., 18, 921-961, 2018.

Artaxo, P., Rizzo, L. V., Brito, J. F., Barbosa, H. M. J., Arana, A., Sena, E. T., Cirino, G. G., Bastos, W., Martin, S. T., and Andreae, M. O.: Atmospheric aerosols in Amazonia and land use change: from natural biogenic to biomass burning conditions, Faraday Discuss, 165, 203-235, 2013.
Bahreini, R., Dunlea, E. J., Matthew, B. M., Simons, C., Docherty, K. S., DeCarlo, P. F., Jimenez, J. L., Brock, C. A., and Middlebrook, A. M.: Design and operation of a pressure-controlled inlet for airborne sampling with an aerodynamic aerosol lens, Aerosol Sci Tech, 42, 465-471, 2008.
Baumgardner, D., Strapp, W., and Dye, J. E.: Evaluation of the Forward Scattering Spectrometer Probe. Part II: Corrections for Coincidence and Dead-Time Losses, 2, 626-632, 1985.
Bhattu, D. and Tripathi, S. N.: CCN closure study: Effects of aerosol chemical composition and mixing state, J Geophys Res-Atmos, 120, 766-783, 2015.
Brenguier, J. L., Bachalo, W. D., Chuang, P. Y., Esposito, B. M., Fugal, J., Garrett, T., Gayet, J. F., Gerber, H., Heymsfield, A., and Kokhanovsky, A.: In situ measurements of cloud and precipitation particles, Airborne Measurements for Environmental Research: Methods and Instruments, 2013. 225-301, 2013.
Broekhuizen, K., Chang, R.-W., Leaitch, W., Li, S.-M., and Abbatt, J.: Closure between measured and modeled cloud condensation nuclei (CCN) using size-resolved aerosol compositions in downtown Toronto, Atmos Chem Phys, 6, 2513-2524, 2006a.
Broekhuizen, K., Chang, R. Y. W., Leaitch, W. R., Li, S. M., and Abbatt, J. P. D.: Closure between measured and modeled cloud condensation nuclei (CCN) using size-resolved aerosol compositions in downtown Toronto, Atmos Chem Phys, 6, 2513-2524, 2006b.
Cai, Y., Montague, D. C., Mooiweer-Bryan, W., and Deshler, T.: Performance characteristics of the ultra high sensitivity aerosol spectrometer for particles between 55 and 800 nm: Laboratory and field studies, J Aerosol Sci, 39, 759-769, 2008.
Chang, R. Y. W., Slowik, J. G., Shantz, N. C., Vlasenko, A., Liggio, J., Sjostedt, S. J., Leaitch, W. R., and Abbatt, J. P. D.: The hygroscopicity parameter (kappa) of ambient organic aerosol at a field site subject to biogenic and anthropogenic influences: relationship to degree of aerosol oxidation, Atmos Chem Phys, 10, 5047-5064, 2010.
Costa, A., Meyer, J., Afchine, A., Luebke, A., Günther, G., Dorsey, J. R., Gallagher, M. W., Ehrlich, A., Wendisch, M., and Baumgardner, D.: Classification of Arctic, midlatitude and tropical clouds in the mixed-phase temperature regime, Atmos Chem Phys, 17, 12219-12238, 2017.
Davidson, E. A., de Araujo, A. C., Artaxo, P., Balch, J. K., Brown, I. F., Bustamante, M. M. C., Coe, M. T., DeFries, R. S., Keller, M., Longo, M., Munger, J. W., Schroeder, W., Soares, B. S., Souza, C. M., and Wofsy, S. C.: The Amazon basin in transition (vol 481, pg 321, 2012), Nature, 483, 232-232, 2012.
DeCarlo, P. F., Kimmel, J. R., Trimborn, A., Northway, M. J., Jayne, J. T., Aiken, A. C., Gonin, M., Fuhrer, K., Horvath, T., Docherty, K. S., Worsnop, D. R., and Jimenez, J. L.: Field-deployable, high-resolution, time-of-flight aerosol mass spectrometer, Anal Chem, 78, 8281-8289, 2006.
Dolgos, G. and Martins, J. V.: Polarized Imaging Nephelometer for in situ airborne measurements of aerosol light scattering, Optics express, 22, 21972-21990, 2014.
Duplissy, J., Gysel, M., Alfarra, M. R., Dommen, J., Metzger, A., Prevot, A. S. H., Weingartner, E., Laaksonen, A., Raatikainen, T., Good, N., Turner, S. F., McFiggans, G., and Baltensperger,

U.: Cloud forming potential of secondary organic aerosol under near atmospheric conditions, Geophys Res Lett, 35, 2008.
Faber, S., French, J. R., and Jackson, R.: Laboratory and in-flight evaluation of measurement uncertainties from a commercial Cloud Droplet Probe (CDP), Atmos Meas Tech, 11, 3645-3659, 2018.
Fan, J., Rosenfeld, D., Zhang, Y., Giangrande, S. E., Li, Z., Machado, L. A., Martin, S. T., Yang, Y., Wang, J., and Artaxo, P.: Substantial convection and precipitation enhancements by ultrafine aerosol particles, Science, 359, 411-418, 2018.
Giez, A., Mallaun, C., Zöger, M., Dörnbrack, A., and Schumann, U.: Static pressure from aircraft trailing-cone measurements and numerical weather-prediction analysis, J Aircraft, 54, 1728-1737, 2017.
Gunthe, S., King, S., Rose, D., Chen, Q., Roldin, P., Farmer, D., Jimenez, J., Artaxo, P., Andreae, M., and Martin, S.: Cloud condensation nuclei in pristine tropical rainforest air of Amazonia: size-resolved measurements and modeling of atmospheric aerosol composition and CCN activity, Atmos Chem Phys, 9, 7551-7575, 2009.
Guyon, P., Boucher, O., Graham, B., Beck, J., Mayol-Bracero, O. L., Roberts, G. C., Maenhaut, W., Artaxo, P., and Andreae, M. O.: Refractive index of aerosol particles over the Amazon tropical forest during LBA-EUSTACH 1999, J Aerosol Sci, 34, 883-907, 2003.
Hermann, M. and Wiedensohler, A. J. J. o. A. S.: Counting efficiency of condensation particle counters at low-pressures with illustrative data from the upper troposphere, 32, 975-991, 2001.
Jaenicke, R. J. J. o. A. S.: The optical particle counter: cross-sensitivity and coincidence, 3, 95-111, 1972.
Jayne, J. T., Leard, D. C., Zhang, X. F., Davidovits, P., Smith, K. A., Kolb, C. E., and Worsnop, D. R.: Development of an aerosol mass spectrometer for size and composition analysis of submicron particles, Aerosol Sci Tech, 33, 49-70, 2000.
Keller, M., Bustamante, M., Gash, J., and Dias, P. S. (Eds.): Amazonia and Global Change, American Geophysical Union, Washington, DC, 2009.
Kleinman, L. I., Daum, P. H., Lee, Y. N., Senum, G. I., Springston, S. R., Wang, J., Berkowitz, C., Hubbe, J., Zaveri, R. A., and Brechtel, F. J.: Aircraft observations of aerosol composition and ageing in New England and Mid-Atlantic States during the summer 2002 New England Air Quality Study field campaign, Journal of Geophysical Research: Atmospheres, 112, 2007.
Klingebiel, M., de Lozar, A., Molleker, S., Weigel, R., Roth, A., Schmidt, L., Meyer, J., Ehrlich, A., Neuber, R., Wendisch, M., and Borrmann, S.: Arctic low-level boundary layer clouds: in situ measurements and simulations of mono- and bimodal supercooled droplet size distributions at the top layer of liquid phase clouds, Atmos Chem Phys, 15, 617-631, 2015.
Krautstrunk, M. and Giez, A.: The transition from FALCON to HALO era airborne atmospheric research. In: Atmospheric Physics, Springer, 2012.
Krisna, T. C., Wendisch, M., Ehrlich, A., Jäkel, E., Werner, F., Weigel, R., Borrmann, S., Mahnke, C., Pöschl, U., Andreae, M. O., Voigt, C., and Machado, L. A. T.: Comparing airborne and satellite retrievals of cloud optical thickness and particle effective radius using a spectral radiance ratio technique: two case studies for cirrus and deep convective clouds, Atmos. Chem. Phys., 18, 4439-4462, 2018.
Kuhn, U., Ganzeveld, L., Thielmann, A., Dindorf, T., Schebeske, G., Welling, M., Sciare, J., Roberts, G., Meixner, F. X., Kesselmeier, J., Lelieveld, J., Kolle, O., Ciccioli, P., Lloyd, J., Trentmann, J., Artaxo, P., and Andreae, M. O.: Impact of Manaus City on the Amazon Green

Ocean atmosphere: ozone production, precursor sensitivity and aerosol load, Atmos Chem Phys, 10, 9251-9282, 2010.
Kulkarni, P. and Wang, J.: New fast integrated mobility spectrometer for real-time measurement of aerosol size distribution - I: Concept and theory, J Aerosol Sci, 37, 1303-1325, 2006a.
Kulkarni, P. and Wang, J.: New fast integrated mobility spectrometer for real-time measurement of aerosol size distribution: II. Design, calibration, and performance characterization, J Aerosol Sci, 37, 1326-1339, 2006b.
Kupc, A., Williamson, C., Wagner, N. L., Richardson, M., and Brock, C. A.: Modification, calibration, and performance of the Ultra-High Sensitivity Aerosol Spectrometer for particle size distribution and volatility measurements during the Atmospheric Tomography Mission (ATom) airborne campaign, Atmos. Meas. Tech., 11, 369-383, 2018.
Lambe, A. T., Onasch, T. B., Massoli, P., Croasdale, D. R., Wright, J. P., Ahern, A. T., Williams, L. R., Worsnop, D. R., Brune, W. H., and Davidovits, P.: Laboratory studies of the chemical composition and cloud condensation nuclei (CCN) activity of secondary organic aerosol (SOA) and oxidized primary organic aerosol (OPOA), Atmos Chem Phys, 11, 8913-8928, 2011.
Lance, S.: Coincidence Errors in a Cloud Droplet Probe (CDP) and a Cloud and Aerosol Spectrometer (CAS), and the Improved Performance of a Modified CDP, J Atmos Ocean Tech, 29, 1532-1541, 2012.
Lance, S., Brock, C. A., Rogers, D., and Gordon, J. A.: Water droplet calibration of the Cloud Droplet Probe (CDP) and in-flight performance in liquid, ice and mixed-phase clouds during ARCPAC, Atmospheric Measurement Techniques, 3, 1683-1706, 2010.
Lawson, R.: Effects of ice particles shattering on the 2D-S probe, Atmos Meas Tech, 4, 1361-1381, 2011.
Lawson, R. P., O'Connor, D., Zmarzly, P., Weaver, K., Baker, B., Mo, Q., and Jonsson, H.: The 2D-S (stereo) probe: Design and preliminary tests of a new airborne, high-speed, high-resolution particle imaging probe, J Atmos Ocean Tech, 23, 1462-1477, 2006.
Liu, B. Y. and Pui, D. Y.: A submicron aerosol standard and the primary, absolute calibration of the condensation nuclei counter, Journal of Colloid and Interface Science, 47, 155-171, 1974.
Long;, C. N., Bucholtz;, A., Jonsson;, H., Schmid;, B., Vogelmann;, A., and Wood, J.: A Method of Correcting for Tilt from Horizontal in Downwelling Shortwave Irradiance Measurements on Moving Platforms, The Open Atmospheric Science Journal, 4, 78-87, 2010.
Luebke, A. E., Afchine, A., Costa, A., Grooss, J. U., Meyer, J., Rolf, C., Spelten, N., Avallone, L. M., Baumgardner, D., and Kramer, M.: The origin of midlatitude ice clouds and the resulting influence on their microphysical properties, Atmos Chem Phys, 16, 5793-5809, 2016.
Martin, S., Artaxo, P., Machado, L., Manzi, A., Souza, R., Schumacher, C., Wang, J., Andreae, M., Barbosa, H., and Fan, J.: Introduction: observations and modeling of the Green Ocean Amazon (GoAmazon2014/5), Atmos Chem Phys, 16, 2016a.
Martin, S. T., Artaxo, P., Machado, L., Manzi, A. O., Souza, R. A. F., Schumacher, C., Wang, J., Biscaro, T., Brito, J., Calheiros, A., Jardine, K., Medeiros, A., Portela, B., de Sa, S. S., Adachi, K., Aiken, A. C., Albrecht, R., Alexander, L., Andreae, M. O., Barbosa, M. J., Buseck, P., Chand, D., Comstock, J. M., Day, D. A., Dubey, M., Fan, J., Fast, J., Fisch, G., Fortner, E., Giangrande, S., Gilles, M., Goldststein, A. H., Guenther, A., Hubbe, J., Jensen, M., Jimenez, J. L., Keutsch, F. N., Kim, S., Kuang, C., Laskskin, A., McKinney, K., Mei, F., Miller, M., Nascimento, R., Pauliquevis, T., Pekour, M., Peres, J., Petaja, T., Pohlker, C., Poschl, U., Rizzo, L., Schmid, B., Shilling, J. E., Dias, M. A. S., Smith, J. N., Tomlmlinson, J. M., Tota, J., and

Wendisch, M.: The Green Ocean Amazon Experiment (Goamazon2014/5) Observes Pollution Affecting Gases, Aerosols, Clouds, and Rainfall over the Rain Forest, B Am Meteorol Soc, 98, 981-997, 2017.
Martin, S. T., Artaxo, P., Machado, L. A. T., Manzi, A. O., Souza, R. A. F., Schumacher, C., Wang, J., Andreae, M. O., Barbosa, H. M. J., Fan, J., Fisch, G., Goldstein, A. H., Guenther, A., Jimenez, J. L., Poschl, U., Dias, M. A. S., Smith, J. N., and Wendisch, M.: Introduction: Observations and Modeling of the Green Ocean Amazon (GoAmazon2014/5), Atmos Chem Phys, 16, 4785-4797, 2016b.
Mei, F., Hayes, P. L., Ortega, A., Taylor, J. W., Allan, J. D., Gilman, J., Kuster, W., de Gouw, J., Jimenez, J. L., and Wang, J.: Droplet activation properties of organic aerosols observed at an urban site during CalNex-LA, J Geophys Res-Atmos, 118, 2903-2917, 2013a.
Mei, F., Setyan, A., Zhang, Q., and Wang, J.: CCN activity of organic aerosols observed downwind of urban emissions during CARES, Atmos Chem Phys, 13, 12155-12169, 2013b.
Middlebrook, A. M., Bahreini, R., Jimenez, J. L., and Canagaratna, M. R.: Evaluation of composition-dependent collection efficiencies for the aerodyne aerosol mass spectrometer using field data, Aerosol Sci Tech, 46, 258-271, 2012.
Minikin, A., Sauer, D., Ibrahim, A., Franke, H., Röschenthaler, T., Fütterer, D. A., and Petzold, A.: The HALO Submicrometer Aerosol Inlet (HASI): Design concept and first characterization, 1st HALO symposium: Airborne Research with HALO: Achievements and Prospects, Oberpfaffenhofen, Deutschland,, 2017. 2017.
Molleker, S., Borrmann, S., Schlager, H., Luo, B., Frey, W., Klingebiel, M., Weigel, R., Ebert, M., Mitev, V., Matthey, R., Woiwode, W., Oelhaf, H., Dornbrack, A., Stratmann, G., Grooss, J. U., Gunther, G., Vogel, B., Muller, R., Kramer, M., Meyer, J., and Cairo, F.: Microphysical properties of synoptic-scale polar stratospheric clouds: in situ measurements of unexpectedly large HNO3-containing particles in the Arctic vortex, Atmos Chem Phys, 14, 10785-10801, 2014.
Olfert, J. S., Kulkarni, P., and Wang, J.: Measuring aerosol size distributions with the fast integrated mobility spectrometer, J Aerosol Sci, 39, 940-956, 2008.
Petzold, A., Marsh, R., Johnson, M., Miller, M., Sevcenco, Y., Delhaye, D., Ibrahim, A., Williams, P., Bauer, H., Crayford, A., Bachalo, W. D., and Raper, D.: Evaluation of Methods for Measuring Particulate Matter Emissions from Gas Turbines, Environ Sci Technol, 45, 3562-3568, 2011.
Pöhlker, M. L., Ditas, F., Saturno, J., Klimach, T., de Angelis, I. H., Araujo, A. C., Brito, J., Carbone, S., Cheng, Y. F., Chi, X. G., Ditz, R., Gunthe, S. S., Holanda, B. A., Kandler, K., Kesselmeier, J., Konemann, T., Kruger, O. O., Lavric, J. V., Martin, S. T., Mikhailov, E., Moran-Zuloaga, D., Rizzo, L. V., Rose, D., Su, H., Thalman, R., Walter, D., Wang, J., Wolff, S., Barbosa, H. M. J., Artaxo, P., Andreae, M. O., Pöschl, U., and Pöhlker, C.: Long-term observations of cloud condensation nuclei over the Amazon rain forest - Part 2: Variability and characteristics of biomass burning, long-range transport, and pristine rain forest aerosols, Atmos Chem Phys, 18, 10289-10331, 2018.
Pöhlker, M. L., Pöhlker, C., Ditas, F., Klimach, T., de Angelis, I. H., Araujo, A., Brito, J., Carbone, S., Cheng, Y. F., Chi, X. G., Ditz, R., Gunthe, S. S., Kesselmeier, J., Konemann, T., Lavric, J. V., Martin, S. T., Mikhailov, E., Moran-Zuloaga, D., Rose, D., Saturno, J., Su, H., Thalman, R., Walter, D., Wang, J., Wolff, S., Barbosa, H. M. J., Artaxo, P., Andreae, M. O., and Poschl, U.: Long-term observations of cloud condensation nuclei in the Amazon rain forest - Part

1: Aerosol size distribution, hygroscopicity, and new model parametrizations for CCN prediction, Atmos Chem Phys, 16, 15709-15740, 2016.
Poschl, U., Martin, S. T., Sinha, B., Chen, Q., Gunthe, S. S., Huffman, J. A., Borrmann, S., Farmer, D. K., Garland, R. M., Helas, G., Jimenez, J. L., King, S. M., Manzi, A., Mikhailov, E., Pauliquevis, T., Petters, M. D., Prenni, A. J., Roldin, P., Rose, D., Schneider, J., Su, H., Zorn, S. R., Artaxo, P., and Andreae, M. O.: Rainforest aerosols as biogenic nuclei of clouds and precipitation in the Amazon, Science, 329, 1513-1516, 2010.
Rissler, J., Swietlicki, E., Zhou, J., Roberts, G., Andreae, M. O., Gatti, L., and Artaxo, P.: Physical properties of the sub-micrometer aerosol over the Amazon rain forest during the wet-to-dry season transition-comparison of modeled and measured CCN concentrations, Atmos Chem Phys, 4, 2119-2143, 2004.
Roberts, G. C., Andreae, M. O., Zhou, J., and Artaxo, P.: Cloud condensation nuclei in the Amazon Basin:"Marine" conditions over a continent?, Geophys Res Lett, 28, 2807-2810, 2001.
Roberts, G. C., Artaxo, P., Zhou, J., Swietlicki, E., and Andreae, M. O.: Sensitivity of CCN spectra on chemical and physical properties of aerosol: A case study from the Amazon Basin, Journal of Geophysical Research: Atmospheres, 107, LBA 37-31-LBA 37-18, 2002.
Rose, D., Gunthe, S., Mikhailov, E., Frank, G., Dusek, U., Andreae, M. O., and Pöschl, U.: Calibration and measurement uncertainties of a continuous-flow cloud condensation nuclei counter (DMT-CCNC): CCN activation of ammonium sulfate and sodium chloride aerosol particles in theory and experiment, Atmos Chem Phys, 8, 1153-1179, 2008.
Salati, E. and Vose, P. B.: Amazon basin: a system in equilibrium, Science, 225, 129-138, 1984.
Schmid, B., Tomlinson, J. M., Hubbe, J. M., Comstock, J. M., Mei, F., Chand, D., Pekour, M. S., Kluzek, C. D., Andrews, E., Biraud, S. C., and Mcfarquhar, G. M.: The Doe Arm Aerial Facility, B Am Meteorol Soc, 95, 723-+, 2014.
Schulz, C., Schneider, J., Amorim Holanda, B., Appel, O., Costa, A., de Sá, S. S., Dreiling, V., Fütterer, D., Jurkat-Witschas, T., Klimach, T., Knote, C., Krämer, M., Martin, S. T., Mertes, S., Pöhlker, M. L., Sauer, D., Voigt, C., Walser, A., Weinzierl, B., Ziereis, H., Zöger, M., Andreae, M. O., Artaxo, P., Machado, L. A. T., Pöschl, U., Wendisch, M., and Borrmann, S.: Aircraft-based observations of isoprene-epoxydiol-derived secondary organic aerosol (IEPOX-SOA) in the tropical upper troposphere over the Amazon region, Atmos. Chem. Phys., 18, 14979-15001, 2018.
Shilling, J. E., Pekour, M. S., Fortner, E. C., Artaxo, P., Sá, S. d., Hubbe, J. M., Longo, K. M., Machado, L. A., Martin, S. T., and Springston, S. R.: Aircraft observations of the chemical composition and aging of aerosol in the Manaus urban plume during GoAmazon 2014/5, Atmos Chem Phys, 18, 10773-10797, 2018.
Shilling, J. E., Zaveri, R. A., Fast, J. D., Kleinman, L., Alexander, M., Canagaratna, M. R., Fortner, E., Hubbe, J. M., Jayne, J. T., and Sedlacek, A.: Enhanced SOA formation from mixed anthropogenic and biogenic emissions during the CARES campaign, Atmos Chem Phys, 13, 2091-2113, 2013.
Thalman, R., de Sa, S. S., Palm, B. B., Barbosa, H. M. J., Pohlker, M. L., Alexander, M. L., Brito, J., Carbone, S., Castillo, P., Day, D. A., Kuang, C. G., Manzi, A., Ng, N. L., Sedlacek, A. J., Souza, R., Springston, S., Watson, T., Pohlker, C., Poschl, U., Andreae, M. O., Artaxo, P., Jimenez, J. L., Martin, S. T., and Wang, J.: CCN activity and organic hygroscopicity of aerosols downwind of an urban region in central Amazonia: seasonal and diel variations and impact of anthropogenic emissions, Atmos Chem Phys, 17, 11779-11801, 2017.

Wang, J.: A fast integrated mobility spectrometer with wide dynamic size range: Theoretical analysis and numerical simulation, J Aerosol Sci, 40, 890-906, 2009.
Wang, J., Krejci, R., Giangrande, S., Kuang, C., Barbosa, H. M., Brito, J., Carbone, S., Chi, X., Comstock, J., Ditas, F., Lavric, J., Manninen, H. E., Mei, F., Moran-Zuloaga, D., Pohlker, C., Pohlker, M. L., Saturno, J., Schmid, B., Souza, R. A., Springston, S. R., Tomlinson, J. M., Toto, T., Walter, D., Wimmer, D., Smith, J. N., Kulmala, M., Machado, L. A., Artaxo, P., Andreae, M. O., Petaja, T., and Martin, S. T.: Amazon boundary layer aerosol concentration sustained by vertical transport during rainfall, Nature, 539, 416-419, 2016.
Wang, J., Lee, Y.-N., Daum, P. H., Jayne, J., and Alexander, M.: Effects of aerosol organics on cloud condensation nucleus (CCN) concentration and first indirect aerosol effect, Atmos Chem Phys, 8, 6325-6339, 2008.
Webster, C. and Freudinger, L.: Interagency Working Group for Airborne Data and Telecommunications, 2018.
Wendisch, M. and Brenguier, J.-L.: Airborne measurements for environmental research: methods and instruments, John Wiley & Sons, 2013.
Wendisch, M., Coe, H., Baumgardner, D., Brenguier, J.-L., Dreiling, V., Fiebig, M., Formenti, P., Hermann, M., Krämer, M., Levin, Z., Maser, R., Mathieu, E., Nacass, P., Noone, K., Osborne, S., Schneider, J., Schütz, L., Schwarzenböck, A., Stratmann, F., and Wilson, J. C.: Aircraft Particle Inlets: State-of-the-Art and Future Needs, B Am Meteorol Soc, 85, 89-92, 2004.
Wendisch, M., Keil, A., and Korolev, A. V.: FSSP characterization with monodisperse water droplets, Journal of Atmospheric and Oceanic Technology, 13, 1152-1165, 1996.
Wendisch, M., Müller, D., Schell, D., and Heintzenberg, J.: An airborne spectral albedometer with active horizontal stabilization, J Atmos Ocean Tech, 18, 1856-1866, 2001.
Wendisch, M., Poschl, U., Andreae, M. O., Machado, L. A. T., Albrecht, R., Schlager, H., Rosenfeld, D., Martin, S. T., Abdelmomonem, A., Afchine, A., Araujo, A. C., Artaxo, P., Aufmhoff, H., Barbosa, H. M. J., Borrmann, S., Braga, R., Buchholz, B., Cecchini, M. A., Costa, A., Curtius, J., Dollner, M., Dorf, M., Dreiling, V., Ebert, V., Ehrlich, A., Ewald, F., Fisch, G., Fix, A., Frank, F., Futterer, D., Heckl, C., Heidelberg, F., Huneke, T., Jakel, E., Jarvinen, E., Jurkat, T., Kanter, S., Kastner, U., Kenntner, M., Kesselmeier, J., Klimach, T., Knecht, M., Kohl, R., Kolling, T., Kramer, M., Kruger, M., Krisna, T. C., Lavric, J. V., Longo, K., Mahnke, C., Manzi, A. O., Mayer, B., Mertes, S., Minikin, A., Molleker, S., Munch, S., Nillius, B., Pfeilsticker, K., Pohlker, C., Roiger, A., Rose, D., Rosenowow, D., Sauer, D., Schnaiter, M., Schneider, J., Schulz, C., de Souza, R. A. F., Spanu, A., Stock, P., Vila, D., Voigt, C., Walser, A., Walter, D., Weigel, R., Weinzierl, B., Werner, F., Yamasoe, M. A., Ziereis, H., Zinner, T., and Zoger, M.: ACRIDICON-CHUVA CAMPAIGN Studying Tropical Deep Convective Clouds and Precipitation over Amazonia Using the New German Research Aircraft HALO, B Am Meteorol Soc, 97, 1885-1908, 2016.
Zaveri, R. A., Berkowitz, C. M., Brechtel, F. J., Gilles, M. K., Hubbe, J. M., Jayne, J. T., Kleinman, L. I., Laskin, A., Madronich, S., and Onasch, T. B.: Nighttime chemical evolution of aerosol and trace gases in a power plant plume: Implications for secondary organic nitrate and organosulfate aerosol formation, NO3 radical chemistry, and N2O5 heterogeneous hydrolysis, Journal of Geophysical Research: Atmospheres, 115, 2010.

1080

Table 1. List of compared measurements and corresponding instruments deployed aboard the G1 and HALO during GoAmazon2014/5. The acronyms are defined in a table at the end of this paper. Dp indicates the particle diameter. ΔDp refers to the size resolution.

Measurement Variables	Instruments deployed on the G1 (Martin et al., 2016; Schmid et al., 2014)	Instruments deployed on HALO (Wendisch et al., 2016)
Static Pressure	Rosemount (1201F1), 0-1400 hPa	Instrumented nose boom tray (DLR development), 0-1400 hPa
Static air temperature	Rosemount E102AL/510BF -50 to +50 °C	Total Air Temperature (TAT) inlet (Goodrich/Rosemount type 102) with an open wire resistance temperature sensor (PT100), -70 to +50 °C
Dewpoint temperature	Chilled mirror hygrometer 1011B -40 to +50 °C	Derived from the water-vapor mixing ratio, which is measured by a tunable diode laser (TDL) system (DLR development), 5-40000 ppmv
3-D wind	Aircraft Integrated Meteorological Measurement System 20 (AIMMS-20)	Instrumented nose boom tray (DLR development) with an air data probe (Goodrich/Rosemount) 858AJ and high-precision Inertial Reference System (IGI IMU-IIe)
Particle number concentration	CPC, cut off size (D_p) =10 nm	CPC, cut off size (D_p) =10 nm
Size distribution*	UHSAS-A, 60-1000 nm.	UHSAS-A, 60-1000 nm.
	FIMS, 20 nm – 500 nm	
Non-Refractory particle chemical composition	HR-ToF-AMS: Organics, Sulfate, Nitrate, Ammonium, Chloride, 60-1000 nm	C-ToF-AMS: Organics, Sulfate, Nitrate, Ammonium, Chloride, 60-1000 nm
CCN concentration	CCN-200, SS= 0.25, 0.5%	CCN-200, SS= 0.13-0.53%
Gas phase concentration	N2O/CO and Ozone Analyzer, CO, O_3 concentration, precision 2 ppb	N2O/CO and Ozone Analyzer, CO, O_3 concentration, precision 2 ppb
Cloud properties*	CDP, 2-50 μm, ΔD_p=1-2 μm	CCP-CDP, 2.5-46 mm, ΔD_p=1-2 μm
	FCDP, 2-50 μm, ΔD_p=1-2 μm	NIXE-CAS: 0.61 -52.5 μm
	2DS, 10-1000 μm	NIXE-CIPgs, 15-960 μm
		CCP-CIPgs: 15-960 μm
Radiation	SPN1 downward irradiance, 400-2700 nm	SMART Albedometer, downward spectral irradiance, 300-2200 nm

***for an individual flight, the size range may vary.**

Table 2. Summary of the total data points compared between the G1 and HALO instruments.

	SEP 9, 2014		SEP 21, 2014	
	G1	HALO	G1	HALO
Atmospheric parameters	2815	2815	7326	12065
Gas phase, CO	N/A	N/A	7326	12065
Gas phase, Ozone	2815	2815	7110	11766
CPC	2043	2043	8466	11646
UHSAS (FIMS)	2031	2031	5841 (9405)	828
AMS	N/A	N/A	587	818
CCNc	663	531	7982	4546
G1: CDP(FCDP) HALO: CCP-CDP (NIXE-CAS)	N/A	N/A	3627(4439)	2051(2260)
G1: 2DS HALO: CCP-CIPgs (NIXE-CIPgs)	N/A	N/A	2280	2261 (2260)
RAD	1355	1355	N/A	N/A

Table 3. Summary of basic statistics of data between in situ measurements on Sep 9.

Comparison of the coordinated flight on Sep. 9										
Variables	G1				HALO					
	min	max	mean	std	min	max	mean	std	slope	R^2
T, K	297.7	300.2	298.9	0.5	297.2	299.4	298.4	0.4	1.002	Neg.
P, hPa	955	965	960.1	1.5	958	964.9	961.8	0.9	0.998	Neg.
WSpd, m/s	0.3	8.9	3.4	1.2	0.3	7.7	3.8	1.1	0.998	Neg.
T_{dew}*, k*	293	296.5	295.0	0.5	292.9	294.9	294.0	0.3	0.996	Neg.
O_3*, ppb*	10.5	58.8	22.2	9.3	18.3	50.8	26.3	6.6	1.082	0.9401
CPC, cm^{-3}	696.0	3480.6	1591.3	568.7	687.4	2639.4	1313.8	473.5	0.819	0.8508
UHSAS, cm^{-3}	78.2	1118.	645.5	116.3	504.1	1622.2	756.3	138.6	1.165	0.8193
CCNc (κ)	0.010	0.347	0.1855	0.067	0.012	0.394	0.1890	0.083	0.8937	Neg.

Table 4 Summary of three statistics analysis of data between in situ measurements on Sep 21

Comparison of the coordinated flight on Sep. 21							
	m	offset	R^2	m0	R^2	m1	R^2
T, K	0.929	20.0	0.9992	0.999	0.9928	0.999	0.9928
P, hPa	1.001	0.929	0.9998	1.001	0.9998	1.001	0.9998
WSpd, m/s	0.885	1.0	0.7875	1.012	0.5076	1.023	0.5049
T_{dew}*, k*	0.989	3.8	0.9963	1.003	0.9904	1.003	0.9904
O_3*, ppb*	1.134	-1.5	0.9598	1.075	0.9369	1.101	0.9208
CO, ppb	0.922	5.4	0.9654	0.966	0.9254	0.967	0.9254
CPC, cm^{-3}	0.571	199.4	0.9482	0.635	0.8738	0.641	0.8735
UHSAS, cm^{-3}	1.126	178.0	0.8249	1.293	0.5070	1.384	0.4847
CCNc (κ)	0.766	55.3	0.8330	0.815	0.6544	0.829	0.6521

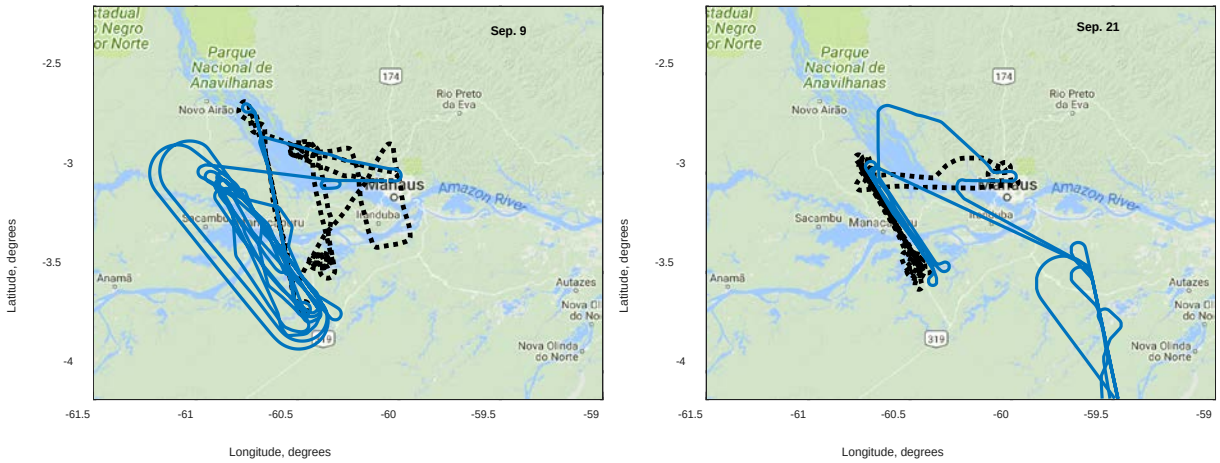

(a) (b)

Figure 1. Coordinated flight tracks for September 9 (a) and September 21 (b). The black dotted line is the flight track of the G1, and the blue line is the flight track of HALO.

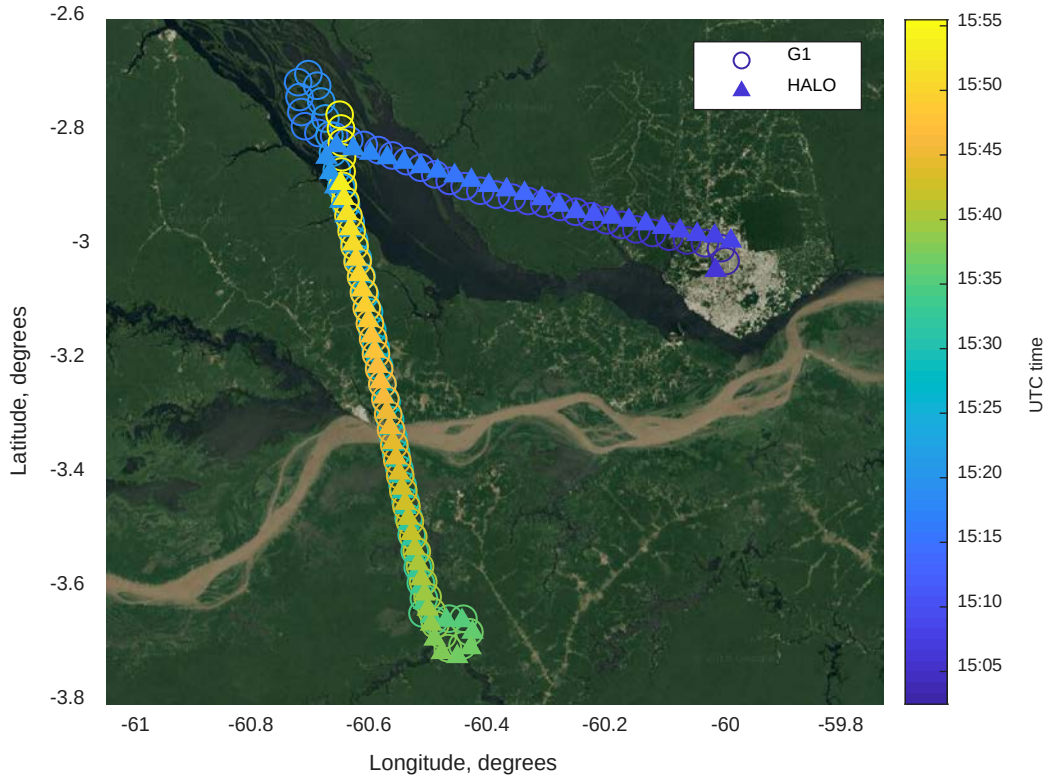

Figure 2. Time-colored flight track of the G1 (circle) and HALO (triangle) on September 9 during a cloud-free coordinated flight at 500 m above sea level (50 m apart as the closest distance).

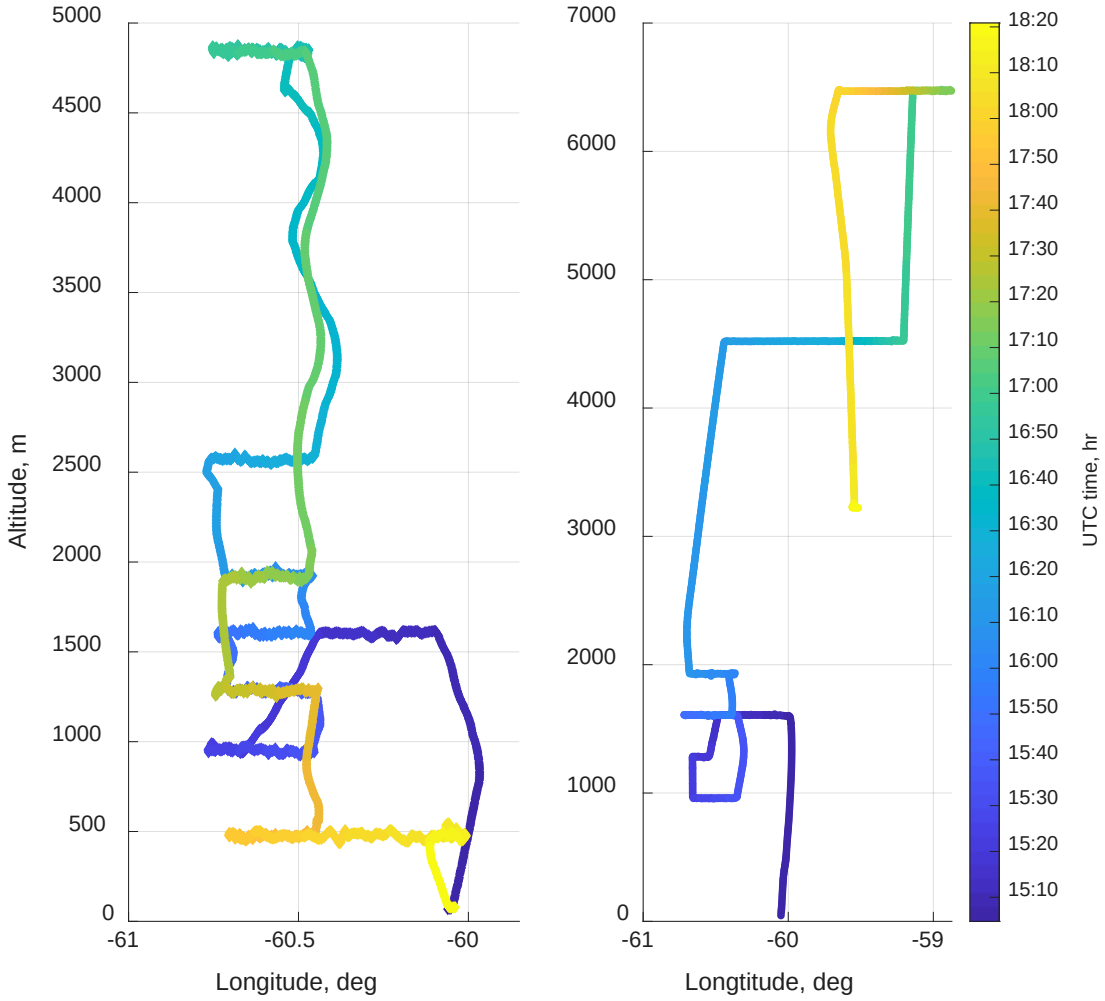

(a) (b)

Figure 3. Time-colored flight profile of the G1 (a) and HALO (b) on September 21, during a coordinated flight.

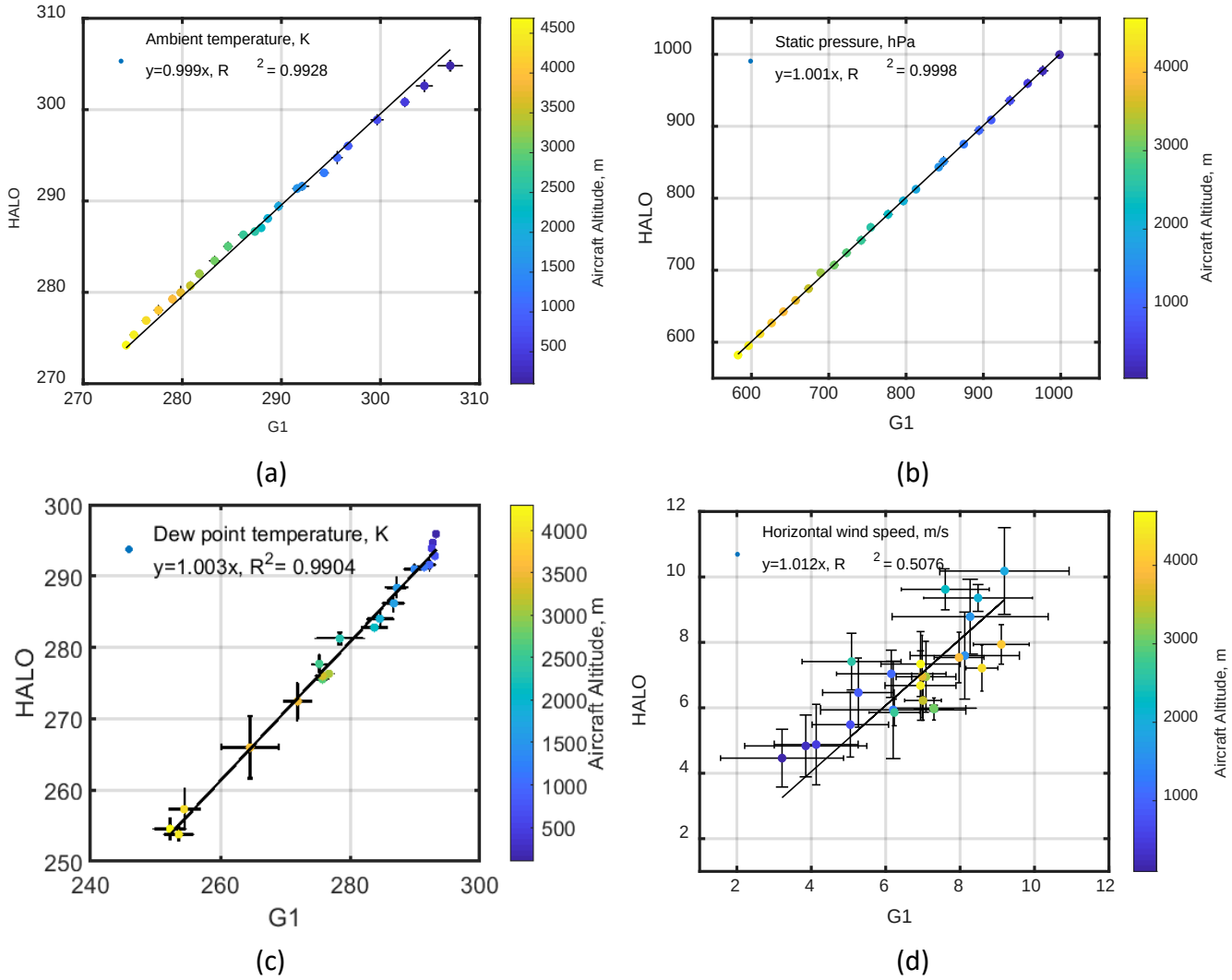

Figure 4. Aircraft altitude-colored plots of (a) ambient temperature, (b) static pressure, (c) dew point temperature, and (d) horizontal wind speed observed by the G1 and HALO on September 21.

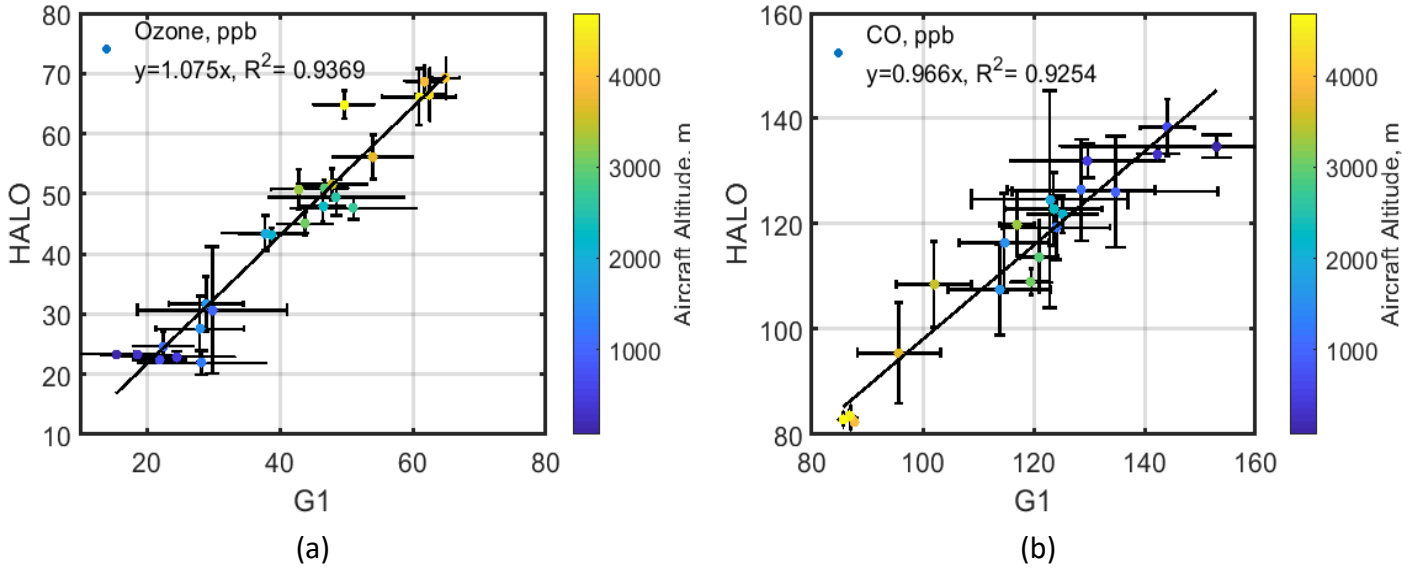

Figure 5. Aircraft altitude-colored plots of trace gas (a) Ozone, (b) CO, for the coordinated flight on September 21.

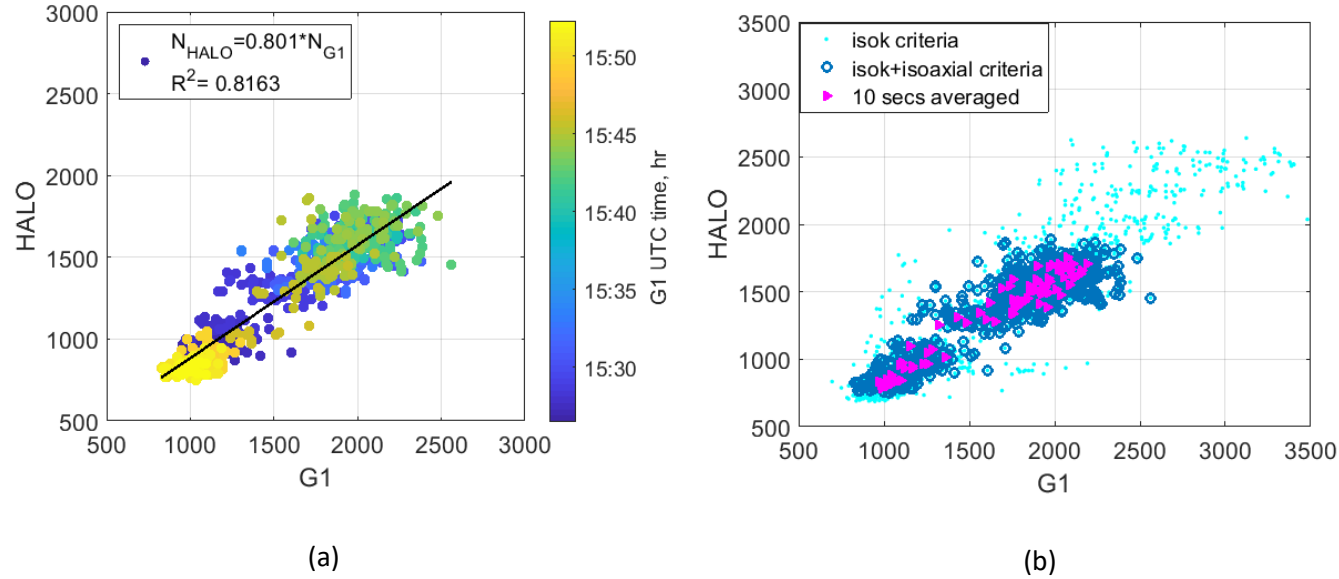

Figure 6. The G1 and HALO comparison for aerosol number concentration measured by CPC (>10 nm) on September 9: (a) with iso-kinetic inlet constrain; (b) with different criteria.

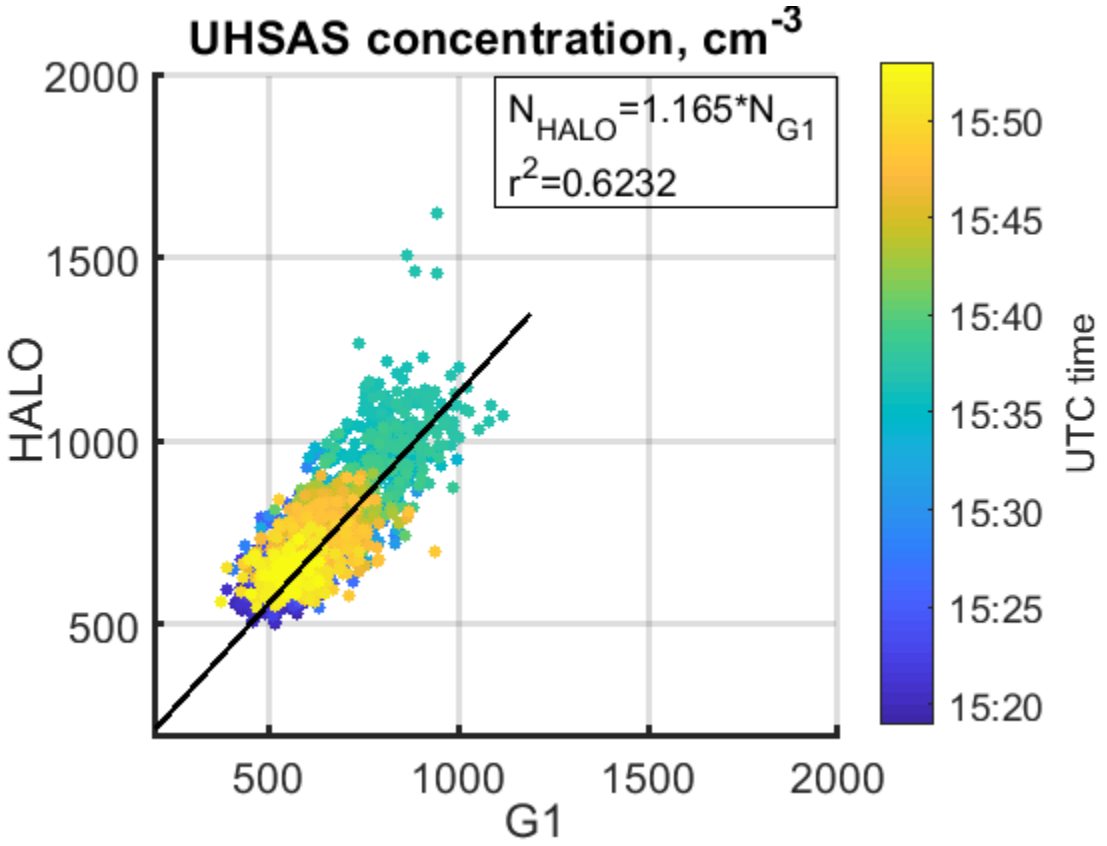

Figure 7. The G1 and HALO comparison for aerosol number concentration measured by UHSAS (90-500 nm) on September 9.

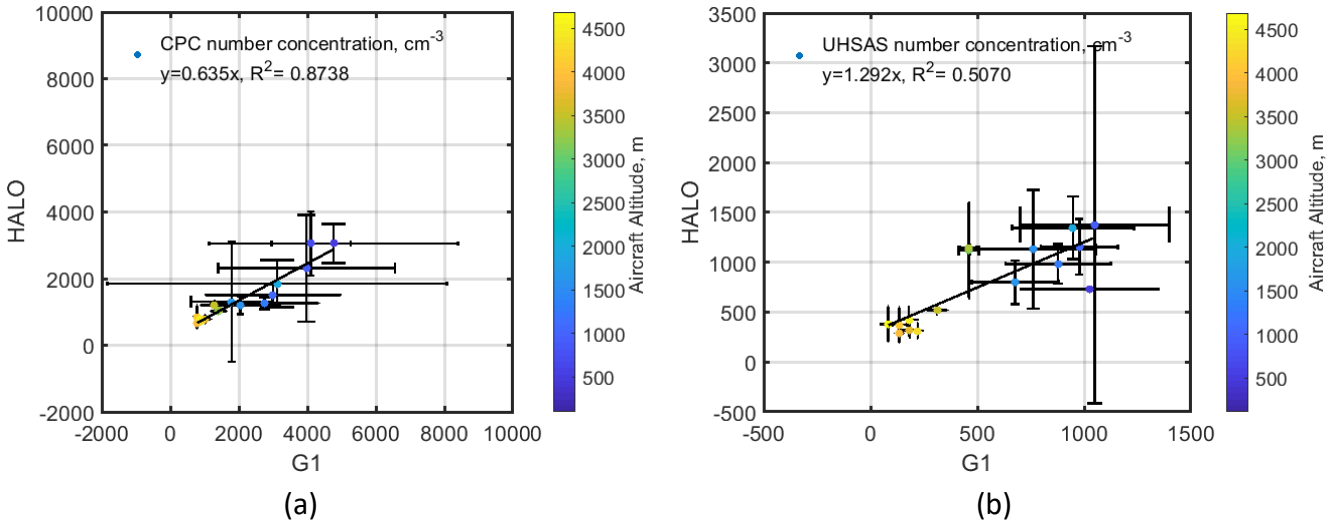

Figure 8. The G1 and HALO comparison for aerosol number concentration profiling measured by (a) CPC and (b) UHSAS (100-700 nm) on September 21.

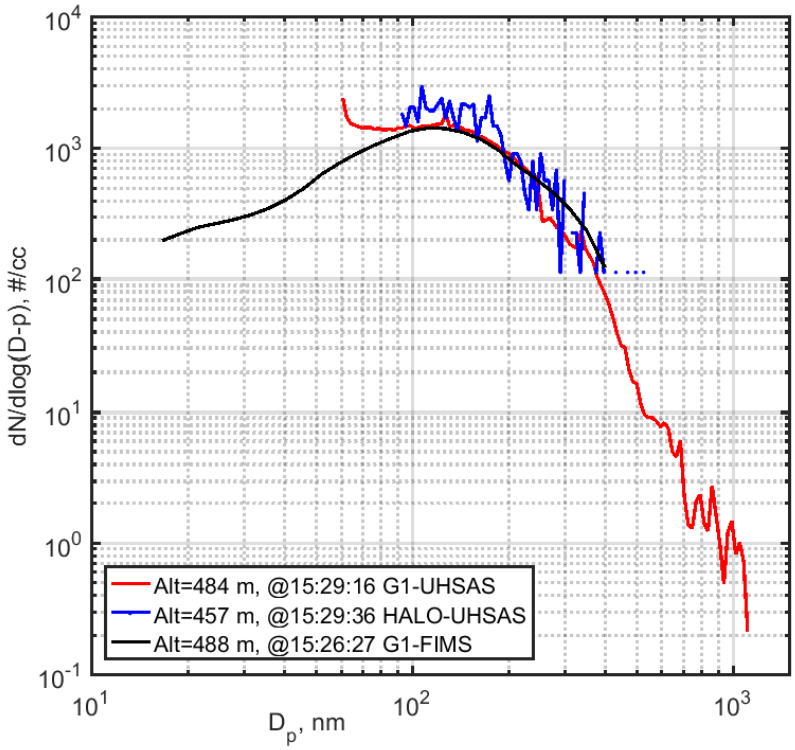

Figure 9. The G1 and HALO comparison for aerosol size distribution measured by UHSAS (from both aircraft) and FIMS (on the G1) on September 9.

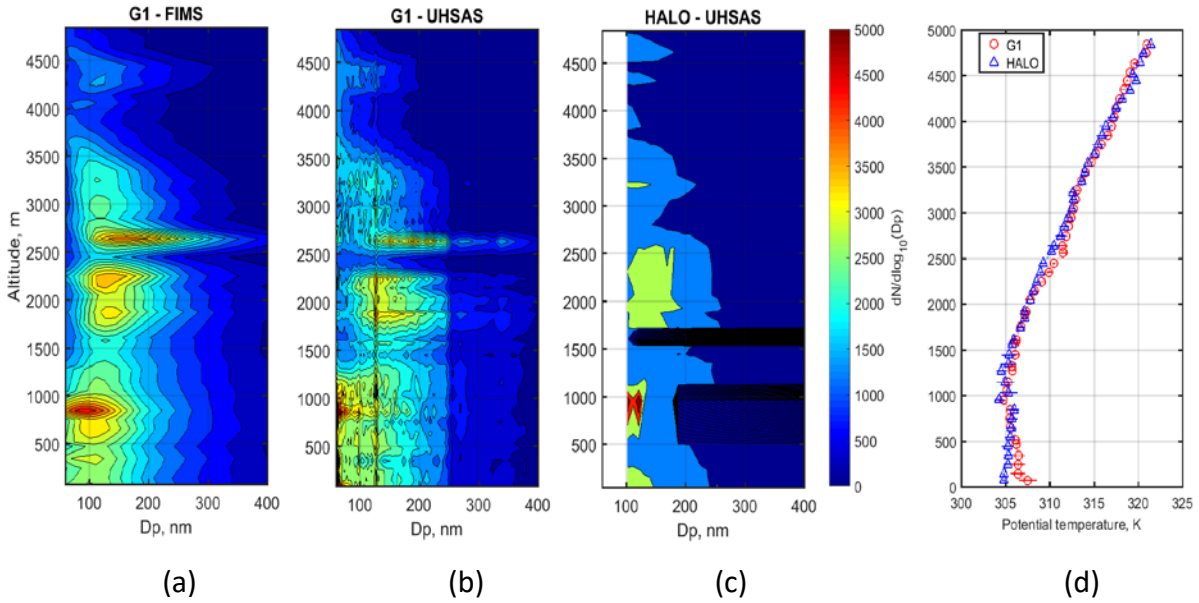

Figure 10. Aerosol size distribution vertical profiles measured by (a) the G1 FIMS, (b) The G1 UHSAS, (c) the HALO UHSAS, (d) Potential temperature aboard the G1 and HALO on September 21.

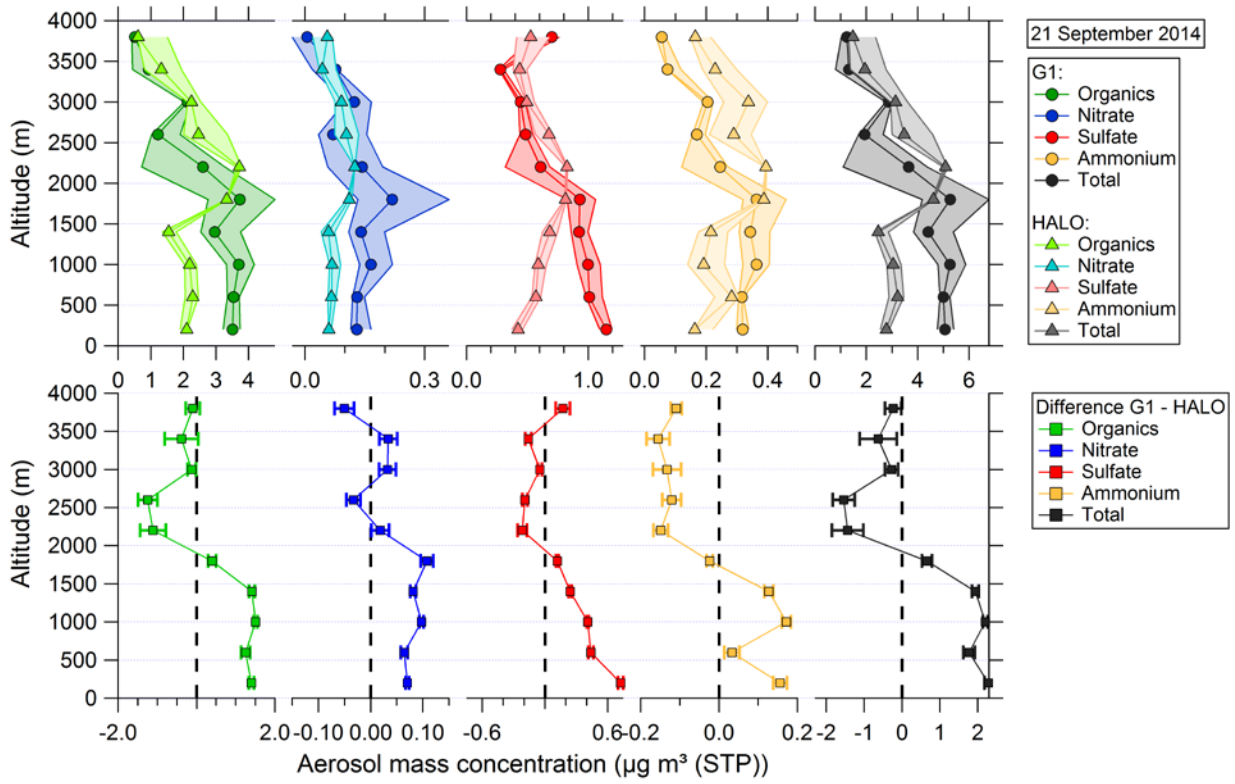

Figure 11. The vertical profile of aerosol mass concentration measured by the G1 and HALO AMS on September 21.

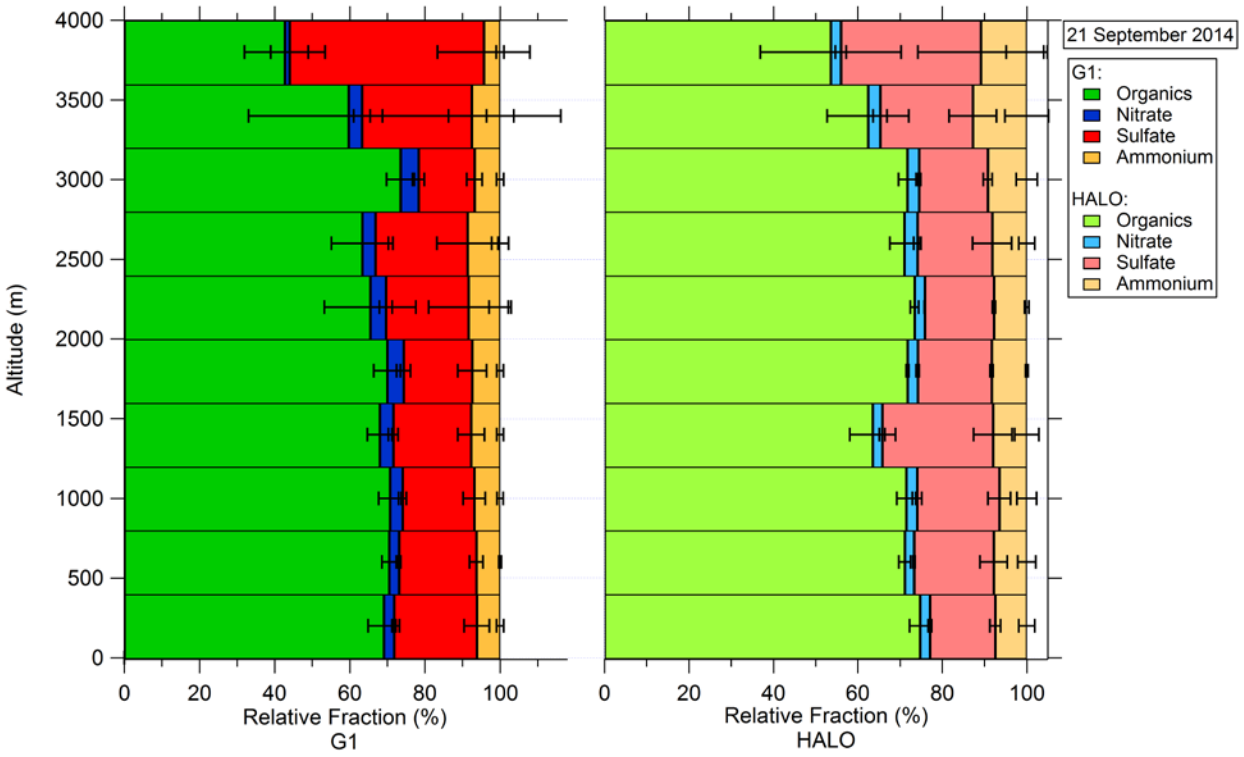

Figure 12. The vertical profile of relative mass fraction of major aerosol chemical species measured by the G1 and HALO AMS, respectively, on September 21

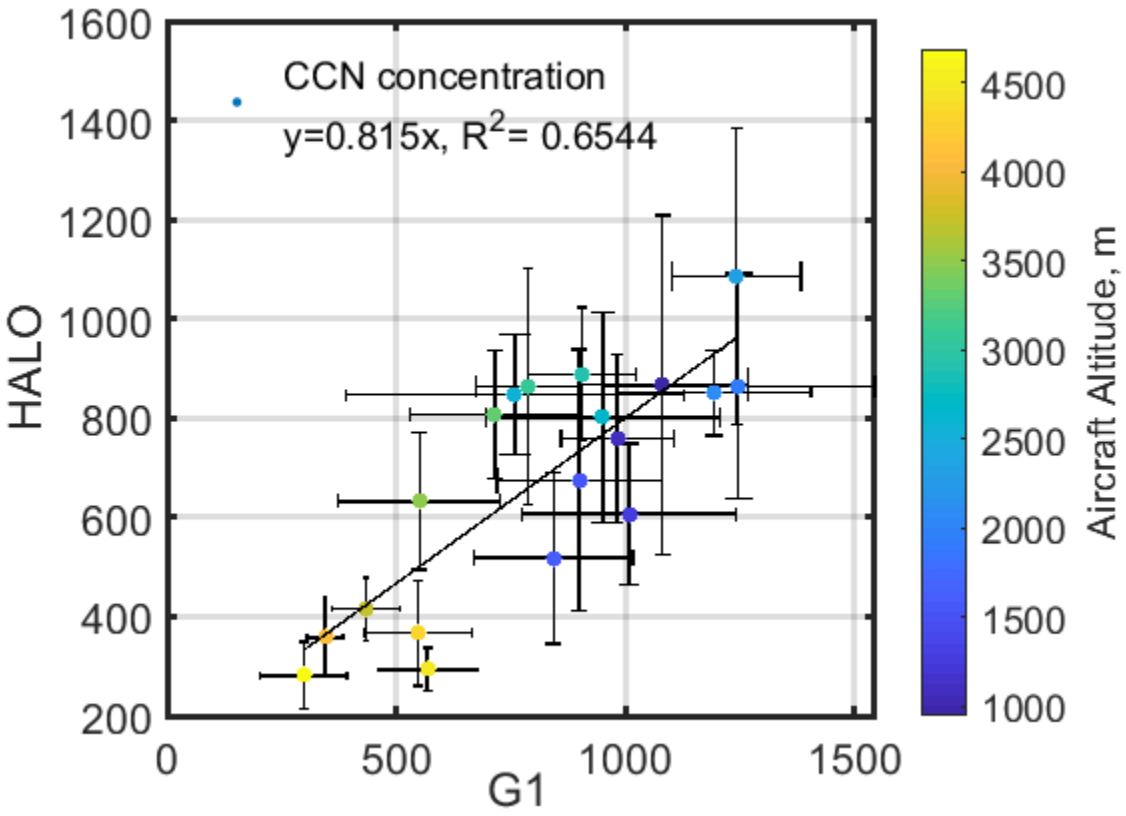

Figure 13. The G1 and HALO comparison of aerosol CCN concentration (S=0.5%) measured on September 21.

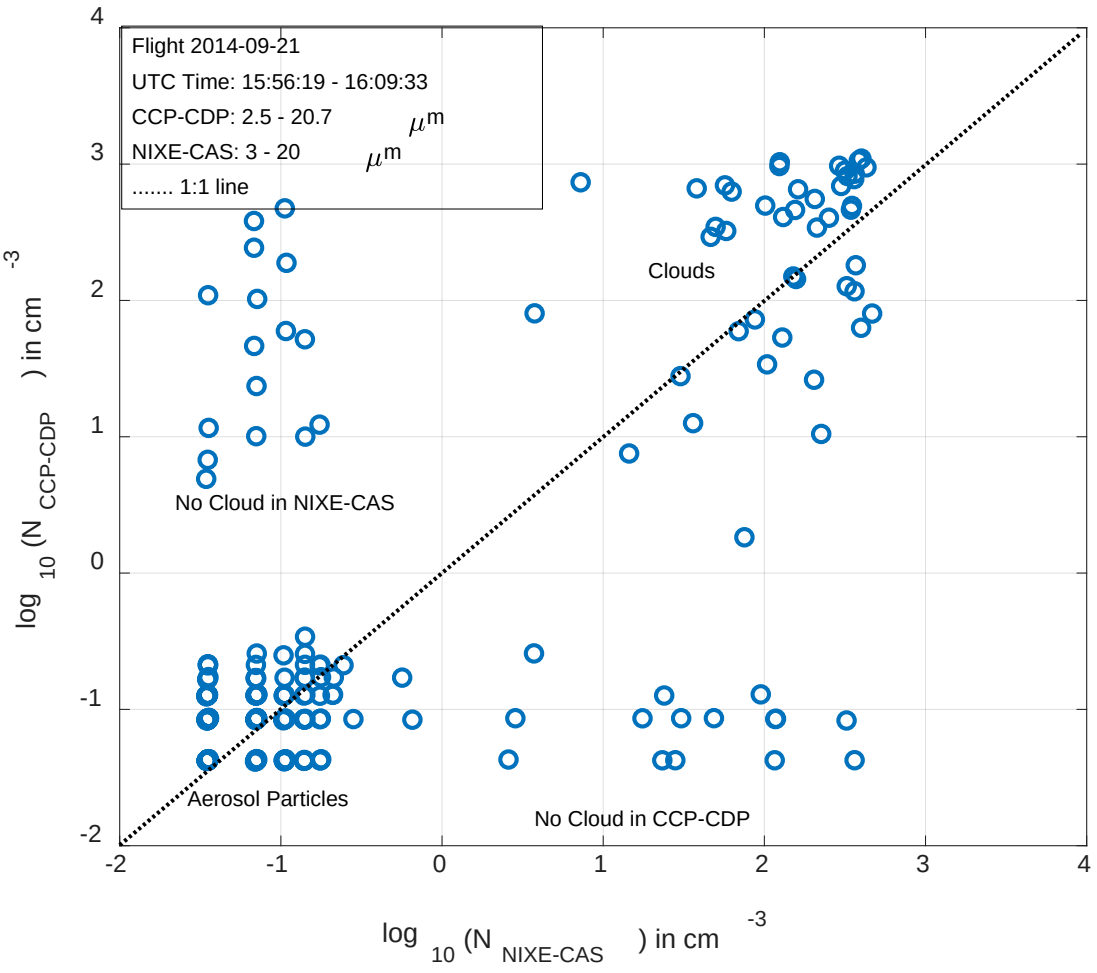
Flight 2014-09-21
UTC Time: 15:56:19 - 16:09:33
CCP-CDP: 2.5 - 20.7 μm
NIXE-CAS: 3 - 20 μm
..... 1:1 line
Clouds
No Cloud in NIXE-CAS
Aerosol Particles
No Cloud in CCP-CDP
log 10 (N CCP-CDP) in cm -3
log 10 (N NIXE-CAS) in cm -3
4
3
2
1
0
-1
-2
-2
-1
0
1
2
3
4

71

72 (a)

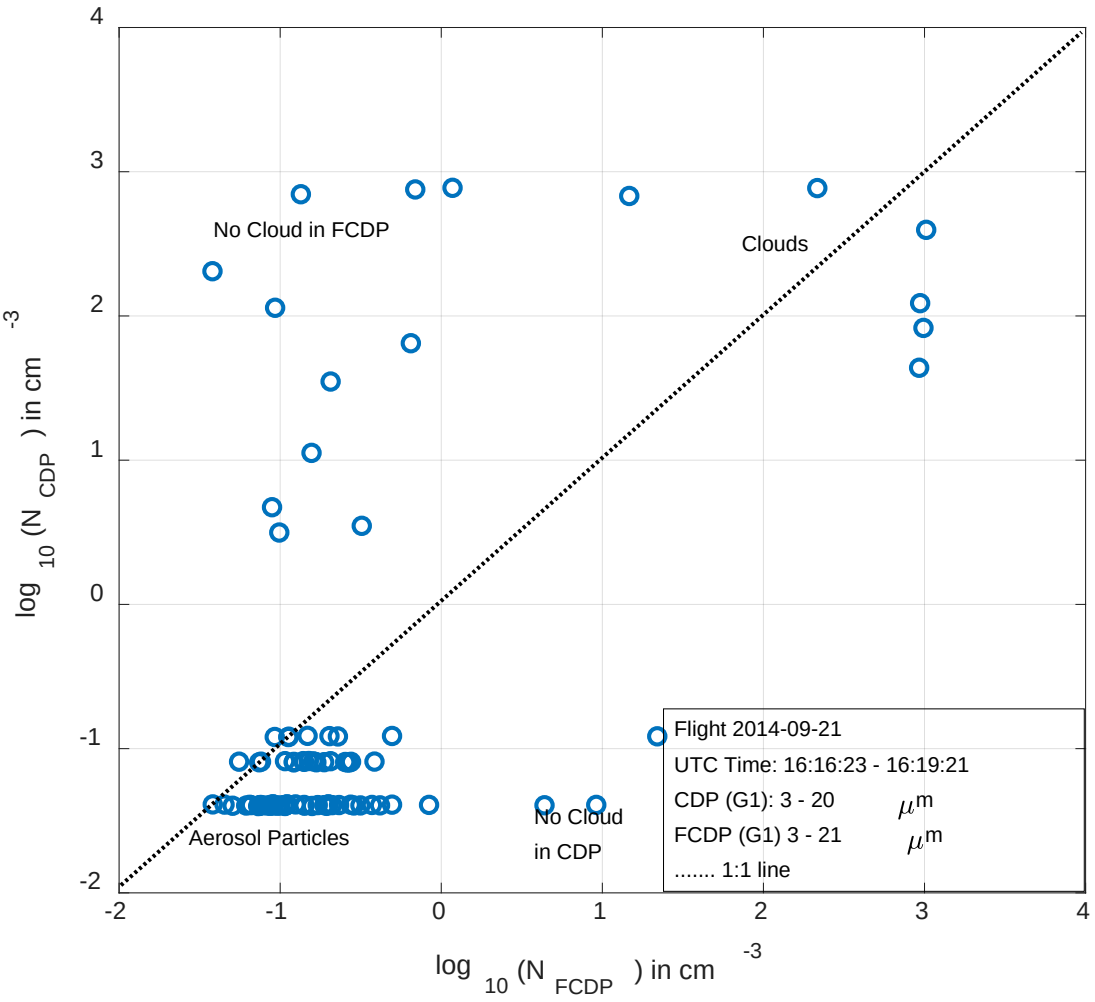

(b)

Figure 14 The comparison of cloud droplet concentrations in the same aircraft (a) between NIXE-CAS and CCP-CDP on board HALO; (b) between CDP and FCDP on board the G1.

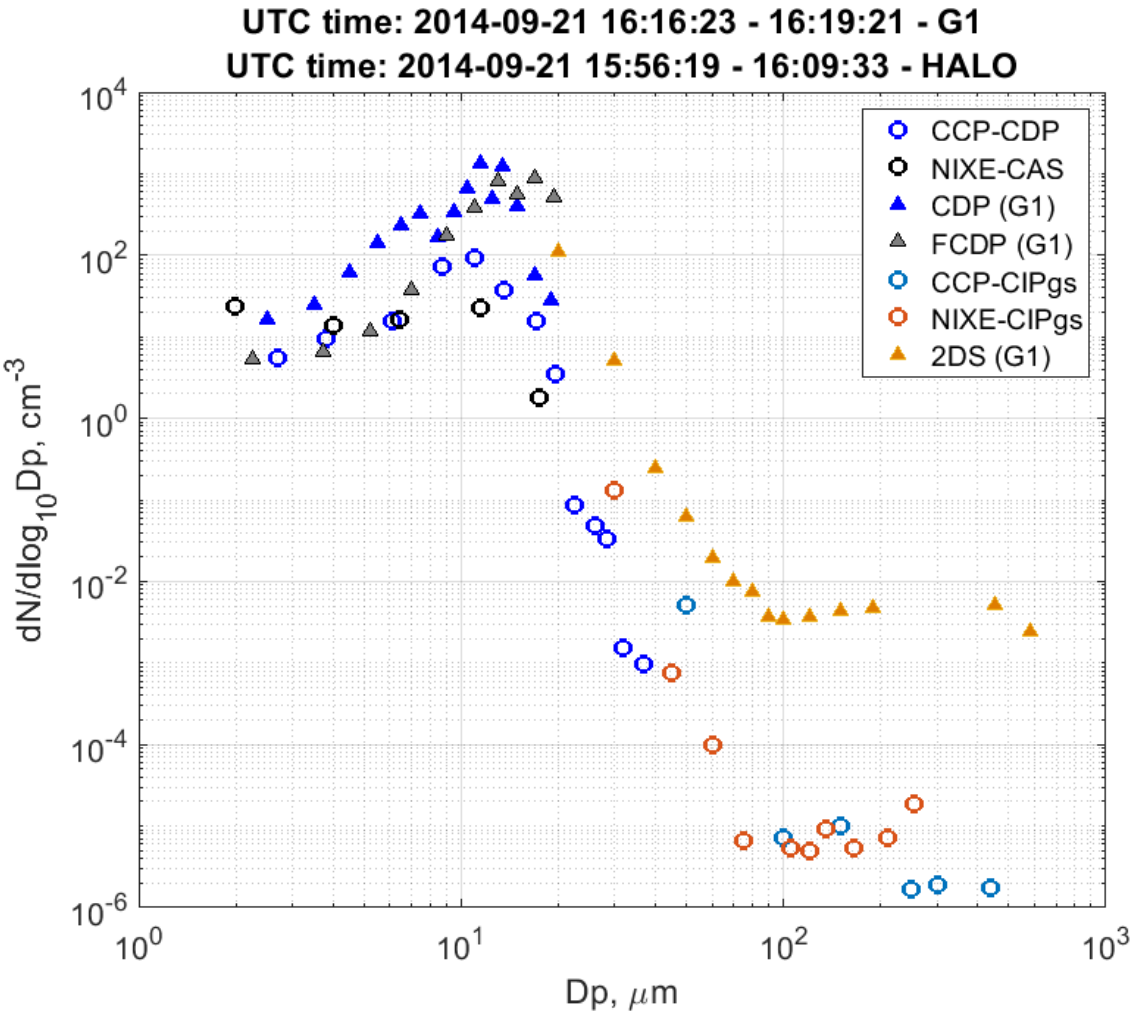

77

78 Figure 15. The cloud droplet size distribution from the cloud probes on the G1 and HALO.

79

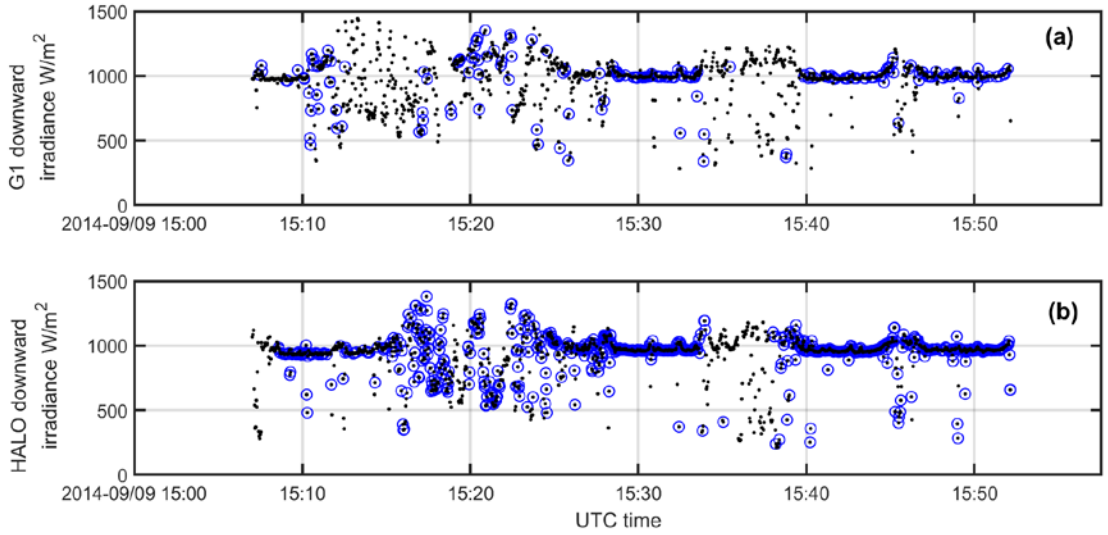

Figure 16. Time series of the G1 and HALO downward irradiance on September 9. The (a) by SPN-1 and (b) by SMART-Albedometer. Black dots represent all data under the general inter-comparison criteria. The blue circles represent the restricted navigation criteria.

Data availability

All ARM datasets used for this study can be downloaded at https://iop.archive.arm.gov/arm-iop/2014/mao/goamazon/ (DOI: 10.5439/1346559). The full data set from the ACRIDICON-CHUVA campaign is archived and publicly accessible from the HALO database maintained by the German Aerospace Center (DLR) at https://halo-db.pa.op.dlr.de/mission/5.

Competing interests

The authors declare that they have no conflict of interest.